



26 Abstract:

27 Organic aerosol (OA) is a major component of fine particulate matter (PM) affecting air quality, human health, and the
28 climate. The absorptive and reflective behavior of OA components contributes to determining particle optical properties and
29 thus their effects on the radiative budget of the troposphere. There is limited knowledge on the influence of the molecular
30 composition of OA on particle optical properties in the polluted urban environment. In this study, we characterized the
31 molecular composition of oxygenated OA collected on filter samples in autumn of 2018 in Beijing, China, with a filter inlet
32 for gases and aerosols coupled to a high-resolution time-of-flight chemical ionization mass spectrometer (FIGAERO-CIMS).
33 Three haze episodes occurred during our sampling period with daily maximum concentrations of OA of 50, 30, and 55 $\mu\text{g m}^{-3}$,
34 respectively. We found that the signal intensities of dicarboxylic acids and sulfur-containing compounds increased during
35 the two more intense haze episodes, while the relative contributions of wood-burning markers and other aromatic compounds
36 were enhanced during the cleaner periods. We further assessed the optical properties of oxygenated OA components by
37 combining the detailed chemical composition measurements with collocated particle light absorption measurements. We show
38 that light-absorption enhancement (E_{abs}) of black carbon (BC) was mostly related to more oxygenated OA (e.g. dicarboxylic
39 acids), likely formed in aqueous-phase reactions during the intense haze periods with higher relative humidity, and speculate
40 that they might contribute to lensing effects. Aromatics and nitro-aromatics (e.g. nitrocatechol and its derivatives) were mostly
41 related to a high light absorption coefficient (b_{abs}) consistent with light-absorbing (brown) carbon (BrC). Our results provide
42 information on oxygenated OA components at the molecular level associated with BrC and BC particle light-absorption and
43 can serve as a basis for further studies on the effects of anthropogenic OA on radiative forcing in the urban environment.

44

45 1. Introduction

46 Organic aerosol (OA) makes up a large fraction of submicron aerosol particles globally (Jimenez et al., 2009). As such, OA
47 plays an essential role in numerous atmospheric processes such as photochemical oxidation, new particle formation and
48 growth, and cloud formation, and influences atmospheric pollution and human health, as well as global radiative forcing
49 (Jimenez et al., 2009; Riipinen et al., 2012; Lu et al., 2019; Lelieveld et al., 2015; Daellenbach et al., 2020). Secondary organic
50 aerosol (SOA) or oxygenated organic aerosol OOA (a surrogate of SOA) comprises a large number of organic compounds,
51 many of them unknown, formed via oxidation of gas-phase organic precursors (volatile organic compounds, VOCs). SOA
52 accounts for a large fraction of the total OA burden in the atmosphere (Jimenez et al., 2009). Knowledge gaps remain regarding
53 SOA sources and formation mechanisms, especially in polluted areas with strong anthropogenic emissions (Huang et al.,
54 2014).

55 OA, is found to be an important source of brown carbon (BrC), as light-absorbing OA is denoted. OA can also act as an
56 effective shell of internally mixed black carbon (BC) particles that focuses photons onto the BC core (named ‘lensing effect’
57 (Jacobson, 2001)), which leads to so-called light-absorption enhancement (E_{abs}) of BC particles (Xie et al., 2019a; Xie et al.,
58 2019b; Zhang et al., 2018; Liu et al., 2015; Wang et al., 2018). For all these optical effects, the chemical composition of OA
59 plays a role (Zhang et al., 2011; Fleming et al., 2020; Laskin et al., 2015); OA light absorption can therefore not be fully
60 quantified based on bulk concentrations only. Certain OA compounds, e.g. nitrophenol derivatives and amorphous carbon
61 spheres (i.e., tarballs), formed from anthropogenic precursors, were found to be important components of BrC (Cheng et al.,
62 2016a; Mohr et al., 2013; Wang et al., 2019b) and to significantly enhance the light absorption properties of particles even
63 when present in small amounts (Teich et al., 2017). In contrast, certain biogenic SOA compounds seem to be less light-
64 absorbing (Zhang et al., 2011). Generally, OA with a higher degree of oxygenation leads to higher BC E_{abs} than less
65 oxygenated OA (Zhang et al., 2018). In fact, less oxygenated OA was estimated to have a negligible or even negative effect
66 on E_{abs} in a study conducted in Beijing, China (Xie et al., 2019a). To better understand the impact of OA composition on
67 particle optical properties, and to estimate effects on radiative forcing on both regional and global scales, detailed OA chemical
68 composition and BrC/BC optical measurements need to be combined.

69 OA components can be characterized at the molecular level using offline gas or liquid chromatography coupled to mass
70 spectrometry (GC/MS or LC/MS), which allows identification and quantification of a limited number or groups of compounds,
71 due to the lack of standards (Schauer et al., 2002; Guo et al., 2012). More recently established online mass spectrometer
72 methods can provide detailed composition information for many OA compounds, albeit without structural information. For



73 example, Aerosol Mass Spectrometers (AMS) are widely used to yield insights into the chemical evolution of OA when
74 combined with factor analytical methods (Cai et al., 2015; Du et al., 2017; Hu et al., 2017; Sun et al., 2016; Jimenez et al., 2009).
75 Mass spectrometers employing chemical ionization coupled with different inlets such as the filter inlet for gases and aerosols
76 (FIGAERO) (Thornton et al., 2020) or the Chemical Analysis of Aerosol Online (CHARON) (Müller et al., 2017) allow for
77 SOA composition analysis in both the gas and particle phase at the molecular level. In addition to online deployments, these
78 mass spectrometers are also used to analyze particles that were collected offline on filters (Siegel et al., 2021; Daellenbach et
79 al., 2016; Huang et al., 2019).

80 In this study, coupled offline filter collection done in Beijing in autumn 2018 and a FIGAERO high-resolution time-of-
81 flight chemical ionization mass spectrometer (FIGAERO-CIMS, Aerodyne Research Inc., US) to investigate (1) OA
82 composition at molecular level during different haze types and (2) its implications for aerosol light-absorptive properties.

83 2. Method

84 2.1 Sampling information

85 The sampling site (39° 56'31" N, 116°17'50" E) is located on the west campus of Beijing University of Chemical
86 Technology (BUCT), which is near the West Third Road in urban Beijing and surrounded by residential areas with local
87 pollution sources such as traffic, residential heating and cooking emissions. The site is located on the top floor of a five-floor
88 building, about 20 m above ground level. Detailed information on the sampling site and its characteristics are reported in
89 previous studies (Kontkanen et al., 2020; Liu et al., 2020b; Cai et al., 2020; Zhou et al., 2020; Kulmala et al., 2021; Yan et al.,
90 2021; Yao et al., 2020). During the sampling period (Nov 3 to Nov 16, 2018), particulate matter with a diameter of 2.5 μm or
91 less (PM_{2.5}) was collected on filters using a four-channel sampler (TH-16A, Tianhong Co., China) with a sampling flow rate
92 of 16.7 L min⁻¹. 12-h PM_{2.5} nighttime (21:30-9:00, the next day) and daytime (9:30-21:00) samples were collected on 47 mm
93 quartz filters (7202, 47mm, Pall Corp., US), pre-baked for 4.5 hours at 550 °C before sampling. The pre-baking time was
94 selected following procedures in a previous study (Liu et al., 2016) to ensure the removal of potential organic contamination.
95 A total of 27 samples (the Nov 6th daytime filter was not analyzed due to a data acquisition error) and 3 blanks were collected
96 (sampling dates are shown in Figure 1 and Table S1). We also conducted detailed comparison between the quartz and Teflon
97 filter samples (presented in Cai et al. in preparation). After sampling, the filters were wrapped in aluminum foil, sealed in a
98 sealing bag and stored in a freezer at -20 °C until analysis.

99 2.2 Offline FIGAERO-CIMS analysis

100 The filters were analyzed using the FIGAERO-CIMS in offline mode (Cai et al., in preparation). In brief, we took punches
101 (2 mm in diameter) of the collected quartz filters and put them between two pre-baked originally sized (25 mm) Zefluor®
102 Teflon filters that fit the FIGAERO filter holder ("sandwich technique"). The particles collected on the filter punch were
103 thermally desorbed by high purity nitrogen gradually heated from room temperature to 200 °C. The desorbed molecules were
104 then charged by addition of iodide (I⁻), which is formed via exposure of methyl iodide to a radioactive source, Po²¹⁰ in this
105 study (Lopez-Hilfiker et al., 2014). The total ion count (TIC) varied between ~600,000 and 1.2 million s⁻¹ during analysis. To
106 avoid depletion of the reagent ion by the large amount of gaseous HNO₃ evaporating even from the small pieces of filter
107 samples at heating temperatures between 80 and 100 °C, a non-uniform temperature ramping procedure was applied (Figure
108 S1): Samples were (1) heated from room temperature (~25 °C) to 60 °C in 8 min, (2) from 60 to 110 °C in 15 min, (3) from
109 110 °C to 200 °C in 12 min, and (4) held at 200 °C for an additional 20 min ("soak"). The analysis protocol, data analysis
110 flow and method characterization are detailed in Cai et al. (in preparation).

111 FIGAERO-CIMS data were analyzed with the Tofware package (v.3.1.0, Tofwerk, Switzerland and Aerodyne, US) within
112 the Igor Pro software (v.7.08, Wavemetrics, US). We identified the molecular composition of 946 ions in the *m/z* range 46 to
113 500 Th. Most of them (939 ions) were clustered with I⁻. The rest were 7 inorganic ions with low molecular weight (NO₂⁻,
114 NO₃⁻, HSO₄⁻, HN₂O₅⁻, NO₆S⁻, H₂NO₇S⁻, H₂N₃O₉⁻) and not considered in the following discussions. Identified CHOX
115 compounds (compounds with molecular composition C_{c>1}, H_{n≥2}, O_{o>1}, X_{0-n}, X can be N, S, or both) were grouped into (1)
116 compounds containing only carbon, hydrogen, and oxygen (CHO, 65±5% of total CHOX signal), (2) nitrogen-containing
117 compounds (CHON, 30±5%), (3), sulfur-containing compounds (CHOS, 5±1%), and (4) compounds containing both nitrogen
118 and sulfur (CHONS, 0.2±0.05%). The time series of the signal intensities of each compound during a heating cycle was
119 normalized to the signal of the reagent ion I⁻. Backgrounds were determined using field blanks, which were scaled by the ratio



120 in signal during the last 1.5–3 min of the soak period of samples and field blanks to account for instrumental backgrounds. A
121 detailed discussion on background determination for offline FIGAERO data can be found in Cai et al. (in preparation). The
122 background-subtracted signal intensities over the entire heating cycle, which includes temperature ramp and soak, were
123 integrated, resulting in a single data point (in total ion counts) per compound and filter sample. Since in this study we focus
124 on the variability of the molecular composition of oxygenated OA and its relative changes, we did not attempt to convert total
125 ion counts into atmospheric concentrations. A discussion on the determination of sensitivity for the FIGAERO offline method
126 is presented in Cai et al. (in preparation).

127 In OA compound analysis, double bond equivalents (DBEs) provide information on the potential number of rings and double
128 bonds in a molecule. DBEs were calculated following the method proposed by Wang et al. (2017), shown as in Eq. (1):

129
$$\text{DBEs} = 1 + c - \frac{1}{2}h + \frac{1}{2}n \quad (1)$$

130 where c , h and n are the number of C, H, and N atoms in the molecular formulae of the corresponding compounds.

131

132 2.3 Collocated measurements and analyses

133 An online Time-of-Flight-Aerosol Chemical Speciation Monitor (ACSM, Aerodyne Research Inc., US) equipped with a
134 $\text{PM}_{2.5}$ lens and standard vaporizer was operated at the same site. In this study, the ionization efficiency (IE, 230 ions pg^{-1}) and
135 relative ionization efficiencies (RIE) for NH_4 (4.0), NO_3 (1.05), SO_4 (0.86) and Cl (1.5) were determined by calibrations with
136 pure standards of ammonium nitrate, ammonium sulfate and ammonium chloride, while the RIE of OA (1.4) was taken from
137 the literature (Canagaratna et al., 2007). A composition-dependent collection efficiency (CE) for ACSM was applied
138 following the method proposed by Middlebrook et al. (2012). Organic carbon (OC) and elemental carbon (EC) of $\text{PM}_{2.5}$ were
139 measured by a semi-continuous OC/EC carbon aerosol analyzer (Model-4, Sunset Laboratory Inc. US) with a time resolution
140 of 1 hour. The instrument was routinely calibrated with a solution of sucrose.

141 Gaseous NH_3 was measured by a collocated nitrate Chemical Ionization–Atmospheric Pressure interface–Time Of Flight
142 mass spectrometer (nitrate CI-APi-TOF, Aerodyne Research Inc., US). Meteorological parameters, including temperature,
143 relative humidity (RH), wind direction and wind speed were measured at the same site. The boundary layer height was
144 calculated by the method proposed by Eresmaa et al. (2012) based on ceilometer (CL-51, Vaisala Inc.) measurements and
145 used to identify the stagnant conditions typical for haze episodes.

146 The aerosol water content (AWC) for the sampling period was calculated with ISORROPIA II (Fountoukis and Nenes, 2007)
147 based on the chemical composition of non-refractory $\text{PM}_{2.5}$ (NR- $\text{PM}_{2.5}$) measured by the ACSM, and gaseous NH_3 .
148 ISORROPIA II was run in forward and metastable modes to achieve stable performance (Wang et al., 2020; Guo et al., 2017).
149 Although uncertainties can arise for aerosol pH calculations due to missing measurements (e.g. HCl and HNO_3 and water-
150 soluble metal cations), we consider our calculations to be robust as the AWC is dominated by RH, temperature and major
151 components of particles (Guo et al., 2017; Guo et al., 2015).

152 Aerosol light absorption measurements were conducted with a multi-wavelength aethalometer (Model AE-33, Magee
153 Scientific Co., US) equipped with a $\text{PM}_{2.5}$ cyclone. The aethalometer measures the optical attenuation (ATN) of light
154 transmitted through PM collected on filters at seven wavelengths (370, 470, 520, 590, 660, 880 and 950 nm) with a time
155 resolution of 5 min. To fill a data gap from Nov 3 to Nov 6 due to calibrations at the BUCT site, we also analyzed the data
156 from another AE-33 located at the Tower Branch of the Institute of Atmospheric Physics (IAP), Chinese Academy of Sciences.
157 The IAP site is located ~6 km northeast of the BUCT site. During the entire month of Nov, the BC analyses agreed well
158 between the two measurement locations ($r = 0.94\text{--}0.95$ and intercept = $0.33\text{--}0.58 \mu\text{g m}^{-3}$ for the 7 wavelengths, Figure S2).

159 2.4 Aerosol optical properties calculations

160 The light absorption coefficient (b_{abs}) is determined from the ATN measured by the aethalometer and corrected for the so-
161 called shadowing effect (Virkkula et al. (2015)), which represents attenuation variation due to high mass loadings on the filter.
162 BC mass concentrations are derived from the shadowing effect-corrected b_{abs} (Hansen et al., 1983).

163 The variation of b_{abs} as a function of wavelength (λ) is described by the Ångström exponent (AAE), which is typically
164 calculated using observations from a pair of wavelengths (Lack and Langridge, 2013) as in Eq. (2):



$$165 \quad \text{AAE} = -\frac{\ln(b_{\text{abs},\lambda_1}) - \ln(b_{\text{abs},\lambda_2})}{\ln(\lambda_1) - \ln(\lambda_2)} \quad (2)$$

166 In this study, we selected the two wavelengths of 370 nm (λ_1) and 880 nm (λ_2) from the aethalometer measurements to
167 calculate the AAE, following previous studies (Wang et al., 2018; Tao et al., 2020; Lim et al., 2014). It has been shown that in
168 contrast to BC, light absorption of BrC has a strong wavelength dependence, which results in high AAE values for BrC (4 to
169 7 (Cheng et al., 2016a)), and much lower AAE values for BC (0.8 to 1.1 (Teich et al., 2017)). An AAE value of 1.0 is generally
170 adopted for BC (AAE_{BC}, (Teich et al., 2017; Xie et al., 2019b; Cheng et al., 2016a) and also used in this study. Here we have
171 used these differences in AAE to separate b_{abs} for BC and BrC following the method by Lack and Langridge (2013). Due to
172 the low absorption of BrC in the infrared and low concentrations of mineral dust in autumn Beijing (Zhang et al., 2013), it
173 can be assumed that b_{abs} at 880 nm is only from BC particles. b_{abs} at 370 nm for BC ($b_{\text{abs},\text{BC},370\text{nm}}$) and BrC ($b_{\text{abs},\text{BrC},370\text{nm}}$) can
174 then be calculated using Eqs. (3) and (4):

$$175 \quad b_{\text{abs},\text{BC},370\text{nm}} = b_{\text{abs},\text{BC},880\text{nm}} \times \left(\frac{370}{880}\right)^{-\text{AAE}_{\text{BC}}} = b_{\text{abs},880\text{nm}} \times \left(\frac{880}{370}\right) \quad (3)$$

$$176 \quad b_{\text{abs},\text{BrC},370\text{nm}} = b_{\text{abs},370\text{nm}} - b_{\text{abs},\text{BC},370\text{nm}} \quad (4)$$

177

178 We note that AAE_{BC} can vary with many factors such as BC core size, coating thickness, morphology, etc. (Zhang et al.,
179 2018; Cheng et al., 2009); BC with a core-shell structure can have an AAE_{BC} higher than 1.0 (Bond and Bergstrom, 2007).
180 We also calculated $b_{\text{abs},\text{BrC},370\text{nm}}$ following the empirical equation method proposed by Wang et al. (2018) using Mie theory
181 calculation and observed a high correlation ($r = 0.98$ and intercept of 1.6 Mm^{-1}) of the time series between the two
182 aforementioned methods.

183 The contribution of BrC to total aerosol absorption at 370nm (P_{BrC}) is assessed by Eq. (5):

$$184 \quad P_{\text{BrC}} = \frac{b_{\text{abs},\text{BrC},370\text{nm}}}{b_{\text{abs},370\text{nm}}} \quad (5)$$

185 Lack and Langridge (2013) postulated that using different values for AAE_{BC} and AAE_{BrC} to attribute aerosol light-absorption
186 to organic and black carbon, respectively, is only valid when there is substantial light absorption contribution ($P_{\text{BC}} > 23\%$)
187 from BrC; the average P_{BrC} in our study period is $34 \pm 9\%$.

188 The light absorption of BC can be enhanced due to the lensing effect (BC absorption enhancement E_{abs}); Jacobson et al.
189 (2001) reported factors of up to 2.9. E_{abs} of BC was calculated here as the ratio of light absorption of BC particles measured
190 at 880 nm by the aethalometer to the theoretical absorption from uncoated pure BC at 880 nm (Eq. (6), (Zhang et al., 2018; Xie
191 et al., 2019a)). The latter is calculated by multiplying EC concentrations (measured by the OC/EC analyzer) by the pure BC
192 mass absorption coefficient (MAC, $7.5 \text{ m}^2/\text{g}$) taken from literature (Bond and Bergstrom, 2007; Wu et al., 2018).

$$193 \quad E_{\text{abs}} = \frac{b_{\text{abs},\text{BC},880\text{nm}}}{b_{\text{abs},\text{pureBC},880\text{nm}}} = \frac{b_{\text{abs},880\text{nm}}}{\text{EC} \times \text{MAC}_{\text{pure,uncoated}}} \quad (6)$$

194

195 3. Results and discussion

196 3.1 Three haze episodes: Temporal variation of PM_{2.5} components and meteorological conditions

197 During the period of sampling, we observed three particulate pollution or haze episodes (visibility $< 10 \text{ km}$ and $\text{RH} < 90\%$
198 (Cai et al., 2020)) with NR-PM_{2.5}+BC concentrations higher than $100 \mu\text{g m}^{-3}$, Nov 3 to 4, Nov 7 to 9 and Nov 11 to 15 (Figure
199 1). Between these episodes, 12-h NR-PM_{2.5}+BC concentrations decreased to $< 15 \mu\text{g m}^{-3}$. During the cleaner days (Nov 5 to
200 Nov 6 and Nov 9 to Nov 10), the OA mass spectra from FIGAERO-CIMS were generally similar (shown in Figure S3). We



201 selected the days of Nov 3 (Ep1), Nov 8 (Ep2), Nov 14 (Ep3) and Nov 10 (clean period) to compare the molecular composition
202 of OA and derive particle optical properties. Even though OA concentrations were similar (Ep1: $49 \mu\text{g m}^{-3}$, Ep2: $30 \mu\text{g m}^{-3}$,
203 Ep3: $40 \mu\text{g m}^{-3}$), the AWC exhibited large differences (Ep1: $65 \mu\text{g m}^{-3}$, Ep2: $12 \mu\text{g m}^{-3}$, Ep3: $263 \mu\text{g m}^{-3}$), indicative of
204 different haze formation mechanisms.

205 Figure 1 shows the time series of temperature, RH, simulated AWC, wind direction and wind speed, as well as the time
206 series of the chemical components during the sampling period. We observed strong diel patterns and a slightly decreasing
207 trend in temperature during the whole sampling period. The wind direction and wind speed did not strongly influence the
208 pollution levels, likely due to the on average relatively low wind speed (0.6 m/s). The ratio of SO_4 to NO_3 (Fig. 1d) was
209 0.47 ± 0.45 , much lower than in the year 2005 ($\text{SO}_4/\text{NO}_3 = 1.6$) in Beijing (Yang et al., 2011), illustrating that nitrate has
210 become a more important PM component due to SO_2 reductions in North China during the last decade. We multiplied the
211 CHOX signals from FIGAERO-CIMS with their corresponding molecular weight to present the total CHOX abundance.
212 Similar temporal variation was observed between CHOX abundance and the OA concentrations from ACSM ($r=0.94$, Figure
213 1(c)).

214 Ep1 and Ep3 were strong haze episodes, with hourly concentrations of $\text{PM}_{2.5}$ of over $200 \mu\text{g m}^{-3}$ and high concentrations of
215 secondary inorganic aerosol (SIA) compounds such as nitrate, ammonium and sulfate. The amplitude of the diurnal cycles of
216 temperature and RH were reduced when $\text{NR-PM}_{2.5+\text{BC}}$ concentrations were larger than $200 \mu\text{g m}^{-3}$ in both episodes. The
217 highest hourly AWC was larger than $100 \mu\text{g m}^{-3}$ and $400 \mu\text{g m}^{-3}$ in Ep1 and Ep3, respectively. In addition to the similarly
218 high RH and AWC, Ep1 and Ep3 were both characterized by the strong influence of air masses arriving from the south of the
219 North China Plain (NCP) (Figure S4). Such conditions are typical for the most severe haze episodes observed in Beijing (Sun
220 et al., 2015; Sun et al., 2013), where high RH and AWC lead to heterogeneous processes and a strong increase of SIA. In Ep1
221 and Ep3, the increase of OA concentrations and f_{44} – the fraction of signal measured by ACSM at mass-to-charge ratio 44 and
222 an indicator of more oxygenated and thus secondary OA (Ng et al., 2011) – shows that not only secondary inorganic but also
223 secondary organic species contributed strongly to those two severe haze episodes (shown in Figure 1)). A complete buildup
224 process of haze was observed in the period of Nov 11 to 15 with Ep3, which seems to occur in two phases: Start of pollution
225 accumulation under relatively dry conditions (Nov 11 – Nov 13), and then the development of haze with high AWC (Nov 13
226 to Nov 14).

227 Ep2 (Nov 8) with the highest hourly $\text{PM}_{2.5}$ concentrations of $150 \mu\text{g m}^{-3}$ was characterized by a prominent OA contribution
228 (43% of $\text{NR-PM}_{2.5+\text{BC}}$) as well as a higher OA to NO_3 ratio (1.5, Figure 1d) compared to Ep1 (24%, 0.50) and Ep3 (27%,
229 0.53), more similar to the cleaner periods during the whole sampling period with $\text{PM}_{2.5} < 35 \mu\text{g m}^{-3}$ (52%, 3.4). In addition,
230 AWC and RH were much lower during Ep2 than during Ep1 and Ep3. This indicates a different haze formation mechanism
231 governing Ep2 compared to Ep1 and Ep3.

232 The clean period (Nov 10) is characterized by low PM and AWC levels, with average $\text{PM}_{2.5}$ and OA concentrations of 14 ± 7
233 $\mu\text{g m}^{-3}$ and $8.4 \pm 4 \mu\text{g m}^{-3}$, respectively. These are much lower than the average values of the whole sampling period (76 ± 79
234 $\mu\text{g m}^{-3}$ and $22 \pm 15 \mu\text{g m}^{-3}$, respectively). During the clean period, the highest value of OA/NO_3 during the sampling period
235 was observed (>10), illustrating the rather small influence of SIA.

236 3.2 Molecular composition of OA

237 The three haze episodes varied in the relative contribution of OA to total $\text{NR-PM}_{2.5+\text{BC}}$, and in the ratio of OA to inorganic
238 species as exemplified by the OA/NO_3 ratio in Figure 1(d). In the following, we examine the molecular composition of OA
239 more closely for the three episodes and the clean period. Figure 2(a) shows the stacked time series of the organic compounds
240 identified by FIGAERO-CIMS and grouped according to their molecular composition into CHO, CHON, CHOS, and CHONS
241 compounds, with the sum of all compounds referred to as CHOX. The time series of the sum of the signal of the CHOX
242 compounds measured by the FIGAERO-CIMS correlates well with that of the OA mass concentrations measured by ACSM
243 ($r = 0.95$), which shows the robustness of our sampling and analysis method. CHO ($65 \pm 5\%$) and CHON ($30 \pm 5\%$) compounds
244 dominated the CHOX signal, even though the relative contributions of the different groups varied between the different
245 episodes. Ep1 and Ep3 showed a high relative contribution of CHO and CHOS compounds (68% and 6.8% for Ep1, and 72%
246 and 7.3% for Ep3, respectively), which can be associated with the rapid formation of oxygenated OA and organosulfates
247 during haze in Beijing (Wang et al., 2021a; Le Breton et al., 2018), and relatively low contribution of CHON compounds (28%
248 and 21% in Ep1 and Ep3, respectively). On the opposite, for the clean period, the relative contributions of CHO and CHOS



249 were lower (56 and 3.4%, respectively), and those of CHON compounds were increased by a factor of ~2 times (40%)
250 compared to Ep1 and Ep3. In Ep2, characterized by low AWC, the CHO compounds had strong signal contributions (73%),
251 similar to Ep1 and Ep3, but much lower contributions of CHOS (3.6%) and a similar contribution of CHON (23%) were
252 observed.

253 For a more detailed look at the molecular composition of compounds during the different episodes, we further subdivided
254 the compounds measured by FIGAERO-CIMS based on their number of carbon atoms per molecule (Figure 2b). In general,
255 during the period analyzed here, compounds with less than 10 carbons contributed most to the total CHOX signal ($78\% \pm 7\%$).
256 Although $<C_{10}$ compounds were dominant, variation of different carbon number compounds was observed for the different
257 periods. In Ep1 and Ep3, the contribution of compounds with low carbon numbers (C_{2-6}) was 83% and 88%, respectively,
258 while in the clean period their fractions went down to 73%. The signal intensities of C_{2-4} compounds were >20 times higher
259 in Ep1 and 3 than the clean period, which is likely related to aqueous phase formation of small molecules (e.g. dicarboxylic
260 acids), as indicated by their high correlation with AWC ($r = 0.86-0.91$). Those small compounds are typically assumed to be
261 formed in the aqueous phase since gas-particle partitioning theory would favor larger precursor ($>C_7$) SOA semi-volatile
262 products in the particle phase (Lim et al., 2010). Another indication of aqueous SOA formation in Ep1 and Ep3 are the f_{44} and
263 f_{43} ratios of ~0.14 and ~0.06, which are within the narrow range of aqueous OA (f_{44} : 0.09–0.16 and f_{43} : ~0.06) observed in a
264 previous study in Beijing (Zhao et al., 2019). In contrast, the relative contributions of $>C_{10}$ compounds were higher in the
265 clean period (36%, compared to Ep3 with 18%), likely attributable to the stronger relative contributions from combustion
266 emissions. In Ep2, C_6 compounds were strongly enhanced (30%) compared to the clean period (18%) and Ep3 (14%), which
267 we associate with organics emitted from biomass burning (discussed below).

268 In Figure 2b we also plot the O:C ratio of CHO group derived from FIGAERO-CIMS data. Similar to what was shown
269 previously for winter of Beijing (Hu et al., 2017; Sun et al., 2016), the bulk O:C generally followed the trend of total OA and
270 total CHOX signal, i.e. higher OA concentrations coincided with more oxygenated OA. The highest O:C values (0.6 to 0.7)
271 were observed during Ep1 and Ep3, while during the clean days, the O:C ratio went down to 0.4 to 0.5. The higher O:C ratios
272 during the haze periods were likely due to the enhanced contribution of SOA. An SOA component related to aqueous-phase
273 processes was found to be a dominant factor for the increase of the degree of oxygenation of OA during a humid pollution
274 period in Beijing (Sun et al., 2016; Zhao et al., 2019). In-cloud or droplet processes may be enhanced and form OA compounds
275 such as small acids (e.g. oxalate) (Guo et al., 2010) and humic-like substances (HULIS) (Laskin et al., 2015). We can therefore
276 expect that the compounds with small carbon numbers that show higher contributions during humid haze periods (e.g. Ep3)
277 may be carboxylic acids and therefore have a relatively high O:C ratio.

278 With secondary OA species being related to smaller carbon number, the temporal variation of the bulk average carbon
279 number was then similar to that of the BC fraction of total $PM_{2.5}$ (f_{BC}) (Figure 2c). BC is a typical indicator of primary
280 combustion emissions (residential heating, traffic exhaust) in Beijing (Cai et al., 2017; Cai et al., 2020; Sandradewi et al.,
281 2008; Zotter et al., 2017). Through secondary formation and oxidation reactions at a later stage of the haze between Nov 11
282 to Nov 15, the contribution of secondary components increased, resulting in a decrease of f_{BC} and H:C ratios, while the O:C
283 ratio increased. In Ep2, BC and f_{BC} increased to $10 \mu\text{g m}^{-3}$ and 9.2% compared to $<2 \mu\text{g m}^{-3}$ and 3.1% on Nov 5 (clean day,
284 the end of Ep1), suggesting that this episode was more influenced by primary emissions rather than secondary formation.
285 Also, the signal of C_6 compounds was increased (shown in Figure 2(b)) due to the increase of $C_6H_{10}O_5I$, which corresponds
286 to anhydrous sugars such as levoglucosan, mannosan, galactosan, and 1,6-anhydro- β -D-glucofuranose from the breakdown
287 of cellulose during wood combustion (Simoneit et al., 1999), tracers for biomass burning activities. Another indicator for
288 biomass burning, f_{60} , representing the fraction of $C_2H_4O^+$ to total OA (Cubison et al., 2011) measured by ACSM, was also
289 increased in Ep2. Ep2 was overall characterized by a larger influence of biomass burning emissions, which is not the case for
290 Ep1 and 3. In Figure S5, we further show the carbon number-segregated O:C ratios during the sampling period, which confirm
291 the different nature of haze episodes 1 and 3 compared to Ep2: the percentage contribution of C_6 compounds to CHO and
292 their O:C ratios were different during Ep2 (42% and 0.8, respectively), compared to 25% (19%) and 0.7 (0.7) for Ep1 (Ep3).

293 The respective roles of different processes such as gas-to-particle conversion and condensed-phase reactions in the increase
294 of OA mass and O:C ratio during the haze episodes can be investigated by looking at the mass increase of carbon, oxygen,
295 and hydrogen in the particle phase separately. As shown in Figure 2(d) and Figure S6, the signal-weighted mass (defined as
296 atom number multiplying their atomic mass) of elements C, H, O, N was generally increased during the three episodes, but
297 the increase in mass concentrations of OA was mainly driven by the addition of both carbon and oxygen, implying that
298 ageing/oxidation reactions (e.g. functionalization of particle-phase organics and aqueous-phase reactions), and gas-to-particle
299 conversion contributed to SOA formation in haze episodes.

300 We also calculated the relative atom fraction of the individual atoms of all CHOX compounds ($f_{\text{atom signal}}$) using Eq. (7):



301

$$f_{\text{atom signal}} = \frac{\sum \text{Signal}_i \times \text{Atom}_{i,j,\text{num}} \times \text{AM}_{i,j}}{\sum \text{Signal}_i \times \text{MW}_i} \quad (7)$$

302

303 Where Signal_i and MW_i represent the signal intensity and molecular weight of compound i , respectively, and $\text{Atom}_{i,j,\text{num}}$ and
304 $\text{AM}_{i,j}$, the number and atomic mass of atom j in compound i , respectively. The time series of $f_{\text{atom signal}}$ is shown in Figure 2
305 (e). Compared to the clean period, a higher $f_{\text{atom signal}}$ of O and slightly lower contributions of C and H were measured in Ep1
306 and Ep3. This indicates again that oxidation reactions play an important role in the increasing total OA mass in the humid
307 haze periods. We can, however, based on this analysis, not make any conclusions about the importance of aqueous-phase
308 reactions. The $f_{\text{atom signal}}$ of N decreased during the haze periods (Ep3: 21%, clean period: 29%) while S increased (Ep3: 1.4%,
309 clean period: 0.67%), consistent with the CHON and CHOS group fraction variations (shown in Figure 2(a)). Although the
310 mechanism of organosulfur and inorganic sulfate formation in heterogeneous reactions is not fully understood, it seems
311 probable that SO_2 is rapidly oxidized and sulfate/organosulfur is formed in aerosol water with different types of oxidants and
catalysts (Song et al., 2018; Cheng et al., 2016b; Liu et al., 2020a; Wang et al., 2021b).

312

313 In the following, we further characterize SOA in the different episodes with respect to: (1) compounds across different
314 carbon and oxygen numbers, (2) compounds with different DBEs and (3) homologous-like series and individual compounds
315 in typical episodes. The distribution of compounds with different carbon and oxygen numbers is shown in Figure 3. During
316 the clean period, the C_6 compounds, especially those with 5 oxygen atoms (and particularly $\text{C}_6\text{H}_{10}\text{O}_5\text{I}^-$), made up 5.9% of all
317 CHO compounds, 70% higher compared to Ep1 and Ep3. This indicates that biomass burning emissions played a relatively
318 more important role during clean periods. Another important characteristic of the clean period was the enhancement of the
319 relative contributions of nitrogen-containing organics, which were dominated by $\text{C}_6\text{H}_n\text{O}_3\text{N}_n$ compounds (possibly
nitrophenols, 5% to CHOX, shown in Figure S7).

320

321 During Ep2, the signals of compounds with 6 carbon and 5 oxygen atoms increased to up to 21% of total CHOX signals,
322 which is a much higher fraction compared to the clean period (5.9%) and haze days (3.5%). Also during Ep2, $\text{C}_6\text{H}_{10}\text{O}_5\text{I}^-$ was
323 the main contributor to this group (shown in Figure S3). The time series of $\text{C}_6\text{H}_{10}\text{O}_5\text{I}^-$ (as well as its fraction of CHOX,
324 $f_{\text{C}_6\text{H}_{10}\text{O}_5\text{I}^-}$) follows the trend of f_{60} measured by the ACSM, and both are strongly enhanced during Ep2 (shown in Figure 2 (b)
325 and Figure S8). The count median diameter (CMD) of the particles was around 60 nm (Figure S4) in Ep2, consistent with
326 fresh biomass burning emissions (50–70 nm during flaming (Vu et al., 2015)), in contrast to the CMD in the clean period (~20
nm) and haze episode Ep3 (~100 nm).

327

328 Ep1 and Ep3 were characterized by higher contributions of compounds with small carbon numbers (<6). Here we show that
329 C_{2-6} compounds with 4 oxygen atoms made up 23% (Ep1) and 27% (Ep3) of the total CHOX, which is 2 and 3 times higher
330 than in Ep2 and the clean period, respectively. Since Ep1 and Ep3 were characterized by lower UVB radiation (shown in
331 Figure S4), high AWC and high f_{44} , this indicates further that these dominant OA compounds with 4 oxygen atoms are
332 dicarboxylic acids, likely formed in aqueous phase reactions. The absolute signal intensity of oxalic acid ($\text{C}_2\text{H}_2\text{O}_4\text{I}^-$) was 50
333 and 70 times higher in Ep1 and Ep3 than in the clean period, and a high correlation was observed between dicarboxylic acids
334 and AWC ($r = \sim 0.75$ for different dicarboxylic acids). As $\text{PM}_{2.5}$ concentrations increased with RH and AWC in Ep3, the
335 concentrations of OA gradually increased from $<10 \mu\text{g m}^{-3}$ (daytime of Nov 11) to over $50 \mu\text{g m}^{-3}$ (nighttime of Nov 13) and
336 the OA molecular composition changed as well. On Nov 11, the signals of C_6 and O_5 compounds were prominent (shown in
337 Figure S9), similar to Ep2 and clean periods. As pollution levels increased, on Nov 12, the contributions of C_{2-6} and O_4
338 compounds strongly increased and the compound distribution became more similar to the haze period (Figure S9), indicative
of the important role of AWC in SOA and severe haze formation in Beijing.

339

340 In order to further characterize organic compounds detected by FIGAERO-CIMS, we plot the Van Krevelen (VK)
341 diagrams of CHO and CHON compounds in Figure 4 and Figure S10, respectively. Each dot in Figure 4 represents a measured
342 OA compound, which is color-coded by the calculated DBE and sized by the square root of its signal. During the clean period,
343 the OA components displayed a higher contribution of unsaturated species ($\text{DBEs} \geq 6$, 11% of total CHOX in the clean period,
344 compared to 7.4% in Ep3) with lower H:C and O:C ratios. Typically, compounds with a DBEs to carbon ratio higher than 0.7
345 are characterized as soot or oxidized polycyclic aromatic hydrocarbons (PAHs) (Cui et al., 2019). The relative contribution
346 of the compounds with carbon number ≥ 6 meeting that criterion was around 12% of the total CHOX signal in clean periods,
347 which was higher compared to Ep3 (7.0%). Figure 4 shows that the compounds with high DBEs generally have between 2
348 and 3 oxygen atoms, implying that they underwent some oxidation. Those compounds with characteristics representative of
349 oxidation products of aromatics (Molteni et al., 2018) exhibit stronger relative contributions during clean periods. For example,
350 the relative intensity of $\text{C}_6\text{H}_6\text{O}_2\text{I}^-$, a benzene (C_6H_6) oxidation product, was around 3 times higher during the clean period.
The relative signal of $\text{C}_7\text{H}_8\text{O}_2\text{I}^-$, formed from toluene (C_7H_8) oxidation, was 40 to 70% higher compared to the haze periods.



351 For the CHON compounds, both the relative contributions of $C_6H_5NO_3I$ (possibly nitrophenol) and $C_7H_7NO_3I$ (possibly
352 methyl nitrophenol) exhibited 2 to 3 times higher relative contributions during clean days than during the haze episodes. The
353 average UVB radiation intensity for the daytime of Nov10 was around 4 times higher than during the haze episodes (shown
354 in Figure S4), which might result in higher levels of OH radicals and a stronger photo-oxidative potential. In addition, the
355 ratio of the signal intensities of nitrophenol to nitrocatechol ($C_6H_5NO_4I$) in clean days was about 5 times higher than during
356 the polluted days of Ep1 and Ep3, also consistent with recent findings in Beijing that the elevated NO_2 during polluted days
357 promotes the formation of nitrocatechols over nitrophenols (Wang et al., 2019b).

358 Generally, for Ep2 we found a number of CHO and CHON compounds reported from laboratory wood-burning ageing
359 experiments and ambient environments strongly influenced by biomass burning emissions (Lin et al., 2012; Mohr et al.,
360 2013; Bertrand et al., 2018; Daellenbach et al., 2019) enhanced compared to the clean period, such as $C_6H_{10}O_5I$ (24 times),
361 $C_6H_5NO_4I$ (33 times) and $C_7H_7NO_4I$ (possibly methyl-nitrocatechol, 7.7 times) (shown in Figure S3). The 72-h back
362 trajectory (air mass retroplume) calculated for Ep2 shows an influence of southern areas at the receptor site, where residential
363 biomass burning emissions are abundant (Figure S4).

364 In Ep1 and 3, substantially higher absolute signals of inorganic ions were observed compared to Ep2 (HNO_3I : 4 times (Ep1)
365 and 3 times (Ep3), SO_3I : 39 times (Ep1) and >500 times (Ep3)) and the clean period (HNO_3I : 43 times (Ep1) and 27 times
366 (Ep3), SO_3I : >200 times (Ep1) and 700 times (Ep3)). As discussed previously, it is worth noting that during heavy haze (Ep1
367 and Ep3), the signals of CH_4SO_3I and $C_2H_4SO_4I$ were much higher than during Ep2 (CH_4SO_3I : 2 times for Ep1 and Ep3,
368 $C_2H_4SO_4I$: 7 times (Ep1) and 8 times (Ep3)) and the clean period ($C_2H_4SO_4I$: 19 times for both Ep1 and Ep3, $C_2H_4SO_4I$: 46
369 times (Ep1) and 58 times (Ep3)). As shown in Figure 4, a homologous-like series of dicarboxylic acids ($C_nH_{2n-4}O_4$) and a
370 series of compounds with one more DBEs ($C_nH_{2n-4}O_4$) were enhanced in Ep1 and Ep3 compared to Ep2. Apart from oxalic
371 acid discussed previously, other dicarboxylic acids such as malonic acid ($C_3H_4O_4I$), succinic acid ($C_4H_6O_4I$), and glutaric
372 acid ($C_5H_8O_4I$) showed much higher (20–60 times) signals compared to the clean period. These findings show that during
373 humid haze in Beijing, a homologous series of dicarboxylic acids, likely formed in the aqueous-phase, may make up a
374 substantial fraction of the more oxygenated OOA (MO-OOA) found in previous studies (Sun et al., 2016). It is also interesting
375 to note that the OA components measured in Ep1 and Ep3 were very similar to those measured at Peking University (PKU),
376 Beijing in winter 2017 during a haze episode with similar $PM_{2.5}$ loadings (PKU: $188 \mu g m^{-3}$) and RH levels (PKU: 74%)
377 (Figure S11, Zheng et al., (in preparation)).

378 In summary, the haze episodes during our sampling period can be classified by two different formation pathways: (1) mainly
379 influenced by relatively fresh biomass burning emissions under low RH with strong OA compound signals of levoglucosan,
380 aromatics and N-containing aromatics, (2) dominated by aqueous-phase reactions with high RH and air masses coming from
381 the south of the NCP with more oxygenated and low molecular weight OA such as dicarboxylic acids. In the next section, we
382 will investigate how the OA compounds formed in different haze types affect aerosol optical properties.

383 3.3 Influence of OA compounds on particle optical properties

384 3.3.1 Temporal variation of b_{abs} and E_{abs}

385 To investigate particle optical properties during the sampling period, we display the time series of AAE, the BrC absorption
386 coefficient, the ratio of BC to EC, and E_{abs} calculated together with OA (Figure 5). The time series of BC and OA generally
387 follow each other, with a stronger diel variation of BC, especially during Ep1 and Ep3 (shown in Figure S4). AAE exhibited
388 an inverse correlation with OA during Ep1 and Ep3, but not Ep2 when biomass burning occurred. Although still higher than
389 during Ep1 and Ep3, the AAE decreased from the end of Ep2 (Nov 9) to the clean period of Nov 10. The average AAE during
390 our sampling period was 1.4, slightly lower than in winter in Beijing (1.6, (Xie et al., 2019b)), likely due to the lower
391 contribution of residential heating activates in autumn than in winter. The variation in AAE throughout the sampling period
392 reflects aerosol optical properties being influenced by the variation of sources, compounds, pollution levels and formation
393 pathways. The temporal evolution of the normalized (to OA) $b_{abs,BrC,370nm}$ is correlated with f_{60} ($r=0.65$) and shows an
394 enhancement during Ep2 and decreases during Ep1 and Ep3 when aqueous-phase reactions may be important. It shows that
395 even though the total OA concentrations and E_{abs} were strongly increased in Beijing during the humid haze, the light-
396 absorption ability of the OA compounds seemed to decrease.

397 During Ep1 and Ep3, E_{abs} was higher than during Ep2, indicating that BC particles were more aged and more thickly coated
398 by organic and inorganic constituents (Figure S12). The lower E_{abs} of the clean period, on the other hand, implies that BC
399 particles were more likely freshly emitted, and therefore less of a potential lensing effect could be observed. Ratios of $PM_{2.5}$
400 major components to EC were used in a previous study to investigate shell effects on BC particles and E_{abs} (Zhang et al.,



2018). Here, we show E_{abs} variation as a function of SIA, POA and SOA to EC ratios (Figure S12). POA and SOA were estimated based on an empirical formula with f_{44} and f_{57} from ACSM measurements as input (Ng et al., 2011). Consistent with earlier work conducted in Paris, France (Zhang et al., 2018), E_{abs} was substantially enhanced with increasing SOA-to-EC ratio (up to 16), while the increase as a function of POA-to-EC and SIA-to-EC ratios was less prominent (shown in Figure S12). SOA thus has the potential to be a more effective shell for BC particles than SIA and POA. The similarity of the AAE, E_{abs} patterns and b_{abs} of different wavelengths from 2 sites ~6 km apart (BUCT and IAP sites, Figure S2) implies that these effects are likely to occur on a regional scale in Beijing. They suggest that light-absorption of BC and BrC particles can be strongly affected by different OA components and that the OA compounds formed in the two haze types have different light-absorption properties.

3.3.2 Correlations between optical parameters and OA compound signals

OA compounds and their potential optical effects are investigated with a correlation analysis in this study. In Figure 6, we show the histograms of the correlation coefficients (r) between the OA compound signals (normalized by EC), E_{abs} (Figure 6 (a)) and $b_{\text{abs,BrC,370nm}}/b_{\text{abs,BC,370nm}}$ (Figure 6 (c)). We normalized OA and $b_{\text{abs,BrC,370nm}}$ since BrC and BC could be co-varied due to the same sources and the influence of meteorology. We selected the 20 OA compounds with the highest r as “key compounds” for E_{abs} of BC and $b_{\text{abs,BrC,370nm}}$ for brown carbon light absorption, respectively. The key compounds for E_{abs} generally exhibited relatively low DBEs (2.3 ± 1.3 for the CHO group and 2.6 ± 1.3 for the CHON group) and high O:C ratios (0.86 ± 0.34 for the CHO group). The much higher O:C ratio of those compounds compared to all CHO compounds (0.48 ± 0.31) indicates that highly oxygenated SOA plays an important role in BC lensing effects and E_{abs} of BC. CHON with 2 to 4 DBEs such as $\text{C}_n\text{H}_{2n-1}\text{NO}_3^-$ and $\text{C}_n\text{H}_{2n-3}\text{NO}_3^-$ (e.g. amine/amides, organonitrites as well as organonitrates) also exhibited a high correlation with E_{abs} . Overall, low MW compounds, CHO with 4 or 5 oxygen atoms and CHON compounds with 3 to 5 oxygen atom, such as $\text{C}_3\text{H}_4\text{O}_4\text{I}$, $\text{C}_3\text{H}_6\text{O}_4\text{I}$, $\text{C}_5\text{H}_6\text{O}_4\text{I}$, $\text{C}_6\text{H}_{10}\text{O}_4\text{I}$, $\text{C}_3\text{H}_5\text{NO}_3\text{I}$, $\text{C}_2\text{H}_3\text{NO}_3\text{I}$, exhibited the highest correlation with E_{abs} at 880 nm, with r of 0.66–0.76. Their time series were similar, with strong enhancement during Ep1 and Ep3 (Figure S13). It has been suggested earlier that MO-OOA could be more important for the BC lensing effect than less oxygenated OOA (LO-OOA) and POA (Zhang et al., 2018). Based on our results we conclude that those small compounds (e.g. dicarboxylic acids) potentially act as important coating shells creating a strong light absorption enhancement for BC during the humid haze events. It should be noted that OA compounds could be both internally or externally mixed with BC-containing particles and thus, the identified OA compounds may not necessarily be coatings on BC particles. Yet, considering the large proportion of BC-containing to total particles during the heating season (60–78%, (Chen et al., 2020)) as well as the large proportion of organics in BC-containing particles in Beijing (60%, (Wang et al., 2019a)), these OA compounds are very likely important components of the BC coating shells with a high potential to increase E_{abs} .

Compared to E_{abs} , the key compounds for $b_{\text{abs,BrC}}$ such as $\text{C}_8\text{H}_8\text{O}_2\text{I}$, $\text{C}_8\text{H}_8\text{O}_3\text{I}$, $\text{C}_5\text{H}_5\text{NOI}$ and $\text{C}_7\text{H}_7\text{NO}_4\text{I}$ in general exhibit higher DBEs (3.4 ± 0.68 for CHO group and 3.9 ± 1.0 for CHON group) and lower O:C ratios (0.32 ± 0.12 for CHO group). These compounds are likely oxidized aromatics and nitro-aromatics. Apart from the aromatic-like compounds, $\text{C}_6\text{H}_{10}\text{O}_5\text{I}$ (e.g. levoglucosan) and $\text{C}_6\text{H}_{12}\text{O}_5\text{I}$ were also found to be moderately correlated with $b_{\text{abs,BrC,370nm}}/b_{\text{abs,BC,370nm}}$, likely due to their co-variation with light-absorbing carbon from biomass burning emissions. The time series of the key compounds for b_{abs} all showed a large enrichment during Ep2 (shown in Figure S13), confirming that biomass burning-related organics (e.g. aromatics) and N-containing organics (e.g. nitrophenol and nitrocatechol derivatives) were important contributors to the light absorption by brown carbon. The correlation coefficient of the normalized OA compounds’ signals and $b_{\text{abs,BrC}}/b_{\text{abs,BC,370nm}}$ was observed to be lower than the normalized signals with E_{abs} . The generally higher correlation for E_{abs} is likely due to the co-varied time series for OA components and E_{abs} during the haze periods.

In summary, we presented a series of OA compounds that have the potential to influence OA light-absorption in two ways in Beijing: (1) during humid haze, more oxygenated OA, with compounds such as dicarboxylic acids likely formed in aqueous phase reactions, have the potential to strongly increase the absorption by BC due to the lensing effect, (2) during haze dominated by fresh biomass burning emissions, compounds with a high number of DBEs and low O numbers, such as aromatics and N-containing aromatics can act as brown carbon and potentially lead to more absorption at shorter wavelengths.

4. Conclusions

Although OA was found earlier to be one of the dominant factors for aerosol optical effects, the chemical composition of OA may act in different roles in aerosol light absorption. To investigate the chemical composition of OA in a polluted



449 megacity and its effects on particle optical properties, in this study for the first time we relied on the molecular composition
450 of OA in autumn Beijing determined by FIGAERO-CIMS. We found that during severe humid haze periods, compounds with
451 a low number of DBEs and high O:C ratios (e.g. dicarboxylic acids) were strongly enhanced. In contrast, during a strong
452 biomass burning episode characterized by low AWC, compounds with a high number of DBEs and low O:C ratio were
453 observed. The comparison between low and high RH haze conditions indicates different mechanisms for haze formation in
454 Beijing, where the former was mainly influenced by local emissions while the latter was governed by secondary components
455 (potentially formed via aqueous-phase reactions) and more influenced by air masses from the southern NCP areas. This
456 implies that in order to reduce pollution in Beijing, the implementation of local direct particle emission control and gaseous
457 precursor emission control in the areas south of Beijing is necessary.

458 By combining the molecular composition of OA with aerosol light-absorption measurements, we found that the compounds
459 that are highly oxygenated, with a low number of carbon atoms and 4 oxygen atoms (e.g. dicarboxylic acids) were strongly
460 increased during humid haze periods and highly correlated with E_{abs} . They are thus likely an important contributor to the
461 coating shells of BC particles and also a potentially important contributor of E_{abs} . Contrarily, the contribution of oxygenated
462 aromatics and nitro-aromatics were found to be closely linked to the light absorption of BrC.

463 In summary, we determined two kinds of haze episodes formed by different mechanisms in autumn Beijing: (1) driven by
464 high AWC and secondary formation, (2) driven by fresh emissions from biomass burning activities. We also determined the
465 OA molecular composition in those two types of episodes and in clean periods, which in turn influenced aerosol optical effects.
466 This is a step forward towards a better understanding of anthropogenic SOA formation in a highly-populated megacity, its
467 impacts on the local climate and its contribution to the air pollution cocktail.

468 *Author contributions*

469 MK, CM, KRD and JC designed the research. JC, CW, CM and KRD analyzed the FIGAERO-CIMS data. JC, JDW, XLF
470 and KRD analyzed the aethalometer data for the BUCT site. JDW and YLS provided aethalometer data for the IAP site. JC,
471 WD, FXZ, SH, XLF, BWC, LY, ZMF, TC, YCL, JTK, TP, JK, PC, DW, JZ, CY, FB, CM, MK and KRD performed the
472 online measurements and interpreted the results. JDW provided the emission inventory for North China and SH provided back
473 trajectory analysis. MK supported and supervised this research. JC, KRD, and CM wrote the manuscript with contributions
474 from all co-authors. All authors have given approval to the final version of this manuscript.

475 *Acknowledgements*

476 This work was supported by ACCC Flagship funded by the Academy of Finland (337549); “Quantifying carbon sink,
477 CarbonSink+ and their interaction with air quality” INAR project funded by Jane and Aatos Erkkö Foundation; European
478 Research Council (ERC) with the projects ATM-GTP (nr. 742206) and CHAPAs (nr. 850614); Knut and Alice Wallenberg
479 Foundation (WAF project CLOUDFORM, grant no. 2017.0165). KRD acknowledges support by the SNF mobility grant
480 P2EZP2_181599

481



482 References

- 483 Bertrand, A., Stefenelli, G., Jen, C. N., Pieber, S. M., Bruns, E. A., Ni, H., Temime-Roussel, B., Slowik, J. G., Goldstein, A.
484 H., El Haddad, I., Baltensperger, U., Prévôt, A. S. H., Wortham, H., and Marchand, N.: Evolution of the chemical fingerprint
485 of biomass burning organic aerosol during aging, *Atmospheric Chemistry and Physics*, 18, 7607-7624, 10.5194/acp-18-7607-
486 2018, 2018.
- 487 Bond, T. C., and Bergstrom, R. W.: Light Absorption by Carbonaceous Particles: An Investigative Review, *Aerosol Science*
488 *and Technology*, 40, 27-67, 10.1080/02786820500421521, 2007.
- 489 Cai, J., Zheng, M., Yan, C., Fu, H.-Y., Zhang, Y.-J., Li, M., Zhou, Z., and Zhang, Y.-H.: Application and Progress of Single
490 Particle Aerosol Time-of-Flight Mass Spectrometry in Fine Particulate Matter Research, *Chinese Journal of Analytical*
491 *Chemistry*, 43, 765-774, 10.1016/S1872-2040(15)60825-8, 2015.
- 492 Cai, J., Wang, J., Zhang, Y., Tian, H., Zhu, C., Gross, D. S., Hu, M., Hao, J., He, K., Wang, S., and Zheng, M.: Source
493 apportionment of Pb-containing particles in Beijing during January 2013, *Environ Pollut*, 226, 30-40,
494 10.1016/j.envpol.2017.04.004, 2017.
- 495 Cai, J., Chu, B., Yao, L., Yan, C., Heikkinen, L. M., Zheng, F., Li, C., Fan, X., Zhang, S., Yang, D., Wang, Y., Kokkonen, T.
496 V., Chan, T., Zhou, Y., Dada, L., Liu, Y., He, H., Paasonen, P., Kujansuu, J. T., Petäjä, T., Mohr, C., Kangasluoma, J., Bianchi,
497 F., Sun, Y., Croteau, P. L., Worsnop, D. R., Kerminen, V.-M., Du, W., Kulmala, M., and Daellenbach, K. R.: Size-segregated
498 particle number and mass concentrations from different emission sources in urban Beijing, *Atmospheric Chemistry and*
499 *Physics*, 20, 12721-12740, 10.5194/acp-20-12721-2020, 2020.
- 500 Cai, J., Daellenbach, R. K., Wu, C., Zheng, F., Du, W., Haslett, S., Kulmala, M., and Mohr, C.: Offline characterization of
501 particulate matter with FIGAERO- CIMS: characterization and best practices, 2021 (to be submitted).
- 502 Canagaratna, M. R., Jayne, J. T., Jimenez, J. L., Allan, J. D., Alfarra, M. R., Zhang, Q., Onasch, T. B., Drewnick, F., Coe, H.,
503 Middlebrook, A., Delia, A., Williams, L. R., Trimborn, A. M., Northway, M. J., DeCarlo, P. F., Kolb, C. E., Davidovits, P.,
504 and Worsnop, D. R.: Chemical and microphysical characterization of ambient aerosols with the aerodyne aerosol mass
505 spectrometer, *Mass Spectrom Rev*, 26, 185-222, 10.1002/mas.20115, 2007.
- 506 Chen, L., Zhang, F., Yan, P., Wang, X., Sun, L., Li, Y., Zhang, X., Sun, Y., and Li, Z.: The large proportion of black carbon
507 (BC)-containing aerosols in the urban atmosphere, *Environmental Pollution*, 263, 114507,
508 <https://doi.org/10.1016/j.envpol.2020.114507>, 2020.
- 509 Cheng, Y., He, K. B., Duan, F. K., Zheng, M., Ma, Y. L., and Tan, J. H.: Measurement of semivolatile carbonaceous aerosols
510 and its implications: a review, *Environ Int*, 35, 674-681, 10.1016/j.envint.2008.11.007, 2009.
- 511 Cheng, Y., He, K.-b., Du, Z.-y., Engling, G., Liu, J.-m., Ma, Y.-l., Zheng, M., and Weber, R. J.: The characteristics of brown
512 carbon aerosol during winter in Beijing, *Atmospheric Environment*, 127, 355-364, 10.1016/j.atmosenv.2015.12.035, 2016a.
- 513 Cheng, Y., Zheng, G., Wei, C., Mu, Q., Zheng, B., Wang, Z., Gao, M., Zhang, Q., He, K., Carmichael, G., Pöschl, U., and
514 Su, H.: Reactive nitrogen chemistry in aerosol water as a source of sulfate during haze events in China, 2, e1601530,
515 10.1126/sciadv.1601530 %J Science Advances, 2016b.
- 516 Cubison, M. J., Ortega, A. M., Hayes, P. L., Farmer, D. K., Day, D., Lechner, M. J., Brune, W. H., Apel, E., Diskin, G. S.,
517 Fisher, J. A., Fuelberg, H. E., Hecobian, A., Knapp, D. J., Mikoviny, T., Riemer, D., Sachse, G. W., Sessions, W., Weber, R.
518 J., Weinheimer, A. J., Wisthaler, A., and Jimenez, J. L.: Effects of aging on organic aerosol from open biomass burning smoke
519 in aircraft and laboratory studies, *Atmospheric Chemistry and Physics*, 11, 12049-12064, 10.5194/acp-11-12049-2011, 2011.
- 520 Cui, M., Li, C., Chen, Y., Zhang, F., Li, J., Jiang, B., Mo, Y., Li, J., Yan, C., Zheng, M., Xie, Z., Zhang, G., and Zheng, J.:
521 Molecular characterization of polar organic aerosol constituents in off-road engine emissions using Fourier transform ion
522 cyclotron resonance mass spectrometry (FT-ICR MS): implications for source apportionment, *Atmospheric Chemistry and*
523 *Physics*, 19, 13945-13956, 10.5194/acp-19-13945-2019, 2019.
- 524 Daellenbach, K. R., Bozzetti, C., Křepelová, A., Canonaco, F., Wolf, R., Zotter, P., Fermo, P., Crippa, M., Slowik, J. G.,
525 Sosedova, Y., Zhang, Y., Huang, R. J., Poulain, L., Szidat, S., Baltensperger, U., El Haddad, I., and Prévôt, A. S. H.:
526 Characterization and source apportionment of organic aerosol using offline aerosol mass spectrometry, *Atmospheric*
527 *Measurement Techniques*, 9, 23-39, 10.5194/amt-9-23-2016, 2016.
- 528 Daellenbach, K. R., Kourtev, I., Vogel, A. L., Bruns, E. A., Jiang, J., Petäjä, T., Jaffrezo, J.-L., Aksoyoglu, S., Kalberer,
529 M., Baltensperger, U., El Haddad, I., and Prévôt, A. S. H.: Impact of anthropogenic and biogenic sources on the seasonal
530 variation in the molecular composition of urban organic aerosols: a field and laboratory study using ultra-high-resolution mass
531 spectrometry, *Atmospheric Chemistry and Physics*, 19, 5973-5991, 10.5194/acp-19-5973-2019, 2019.
- 532 Daellenbach, K. R., Uzu, G., Jiang, J., Cassagnes, L.-E., Leni, Z., Vlachou, A., Stefenelli, G., Canonaco, F., Weber, S., Segers,
533 A., Kuenen, J. J. P., Schaap, M., Favez, O., Albinet, A., Aksoyoglu, S., Dommen, J., Baltensperger, U., Geiser, M., El Haddad,
534 I., Jaffrezo, J.-L., and Prévôt, A. S. H.: Sources of particulate-matter air pollution and its oxidative potential in Europe, *Nature*,
535 587, 414-419, 10.1038/s41586-020-2902-8, 2020.



- 536 Du, W., Zhao, J., Wang, Y. Y., Zhang, Y. J., Wang, Q. Q., Xu, W. Q., Chen, C., Han, T. T., Zhang, F., Li, Z. Q., Fu, P. Q.,
537 Li, J., Wang, Z. F., and Sun, Y. L.: Simultaneous measurements of particle number size distributions at ground level and
538 260m on a meteorological tower in urban Beijing, China, *Atmospheric Chemistry and Physics*, 17, 6797-6811, 10.5194/acp-
539 17-6797-2017, 2017.
- 540 Eresmaa, N., Härkönen, J., Joffre, S. M., Schultz, D. M., Karppinen, A., and Kukkonen, J.: A Three-Step Method for
541 Estimating the Mixing Height Using Ceilometer Data from the Helsinki Testbed, *Journal of Applied Meteorology and
542 Climatology*, 51, 2172-2187, 10.1175/jamc-d-12-058.1, 2012.
- 543 Fleming, L. T., Lin, P., Roberts, J. M., Selimovic, V., Yokelson, R., Laskin, J., Laskin, A., and Nizkorodov, S. A.: Molecular
544 composition and photochemical lifetimes of brown carbon chromophores in biomass burning organic aerosol, *Atmospheric
545 Chemistry and Physics*, 20, 1105-1129, 10.5194/acp-20-1105-2020, 2020.
- 546 Fountoukis, C., and Nenes, A.: ISORROPIA II: a computationally efficient thermodynamic equilibrium model for
547 K^{+} – Ca^{2+} – Mg^{2+} – NH_4^{+} – Na^{+} – SO_4^{2-} – NO_3^{-} – Cl^{-} – H_2O aerosols, *Atmos. Chem. Phys.*, 7, 4639-4659, 10.5194/acp-7-4639-2007,
548 2007.
- 549 Guo, H., Xu, L., Bougiatioti, A., Cerully, K. M., Capps, S. L., Hite, J. R., Carlton, A. G., Lee, S. H., Bergin, M. H., Ng, N.
550 L., Nenes, A., and Weber, R. J.: Fine-particle water and pH in the southeastern United States, *Atmospheric Chemistry and
551 Physics*, 15, 5211-5228, 10.5194/acp-15-5211-2015, 2015.
- 552 Guo, H., Liu, J., Froyd, K. D., Roberts, J. M., Veres, P. R., Hayes, P. L., Jimenez, J. L., Nenes, A., and Weber, R. J.: Fine
553 particle pH and gas–particle phase partitioning of inorganic species in Pasadena, California, during the 2010 CalNex campaign,
554 *Atmospheric Chemistry and Physics*, 17, 5703-5719, 10.5194/acp-17-5703-2017, 2017.
- 555 Guo, S., Hu, M., Wang, Z. B., Slanina, J., and Zhao, Y. L.: Size-resolved aerosol water-soluble ionic compositions in the
556 summer of Beijing: implication of regional secondary formation, *Atmos. Chem. Phys.*, 10, 947-959, 10.5194/acp-10-947-
557 2010, 2010.
- 558 Guo, S., Hu, M., Guo, Q., Zhang, X., Zheng, M., Zheng, J., Chang, C. C., Schauer, J. J., and Zhang, R.: Primary Sources and
559 Secondary Formation of Organic Aerosols in Beijing, China, *Environmental Science & Technology*, 46, 9846-9853,
560 10.1021/es2042564, 2012.
- 561 Hansen, A., Rosen, H., and Novakov, T.: Aethalometer—an instrument for the real-time measurement of optical absorption by
562 aerosol particles, Lawrence Berkeley Lab., CA (USA), 1983.
- 563 Hu, W., Hu, M., Hu, W. W., Zheng, J., Chen, C., Wu, Y. S., and Guo, S.: Seasonal variations in high time-resolved chemical
564 compositions, sources, and evolution of atmospheric submicron aerosols in the megacity Beijing, *Atmospheric Chemistry and
565 Physics*, 17, 9979-10000, 10.5194/acp-17-9979-2017, 2017.
- 566 Huang, R. J., Zhang, Y., Bozzetti, C., Ho, K. F., Cao, J. J., Han, Y., Daellenbach, K. R., Slowik, J. G., Platt, S. M., Canonaco,
567 F., Zotter, P., Wolf, R., Pieber, S. M., Bruns, E. A., Crippa, M., Ciarelli, G., Piazzalunga, A., Schwikowski, M., Abbaszade,
568 G., Schnelle-Kreis, J., Zimmermann, R., An, Z., Szidat, S., Baltensperger, U., El Haddad, I., and Prevot, A. S.: High secondary
569 aerosol contribution to particulate pollution during haze events in China, *Nature*, 514, 218-222, 10.1038/nature13774, 2014.
- 570 Huang, W., Saathoff, H., Shen, X., Ramisetty, R., Leisner, T., and Mohr, C.: Seasonal characteristics of organic aerosol
571 chemical composition and volatility in Stuttgart, Germany, *Atmospheric Chemistry and Physics*, 19, 11687-11700,
572 10.5194/acp-19-11687-2019, 2019.
- 573 Jacobson, M. Z.: Strong radiative heating due to the mixing state of black carbon in atmospheric aerosols, *Nature*, 409, 695-
574 697, 10.1038/35055518, 2001.
- 575 Jimenez, J. L., Canagaratna, M. R., Donahue, N. M., Prevot, A. S., Zhang, Q., Kroll, J. H., DeCarlo, P. F., Allan, J. D., Coe,
576 H., Ng, N. L., Aiken, A. C., Docherty, K. S., Ulbrich, I. M., Grieshop, A. P., Robinson, A. L., Duplissy, J., Smith, J. D.,
577 Wilson, K. R., Lanz, V. A., Hueglin, C., Sun, Y. L., Tian, J., Laaksonen, A., Raatikainen, T., Rautiainen, J., Vaattovaara, P.,
578 Ehn, M., Kulmala, M., Tomlinson, J. M., Collins, D. R., Cubison, M. J., Dunlea, E. J., Huffman, J. A., Onasch, T. B., Alfarra,
579 M. R., Williams, P. I., Bower, K., Kondo, Y., Schneider, J., Drewnick, F., Borrmann, S., Weimer, S., Demerjian, K., Salcedo,
580 D., Cottrell, L., Griffin, R., Takami, A., Miyoshi, T., Hatakeyama, S., Shimono, A., Sun, J. Y., Zhang, Y. M., Dzepina, K.,
581 Kimmel, J. R., Sueper, D., Jayne, J. T., Herndon, S. C., Trimborn, A. M., Williams, L. R., Wood, E. C., Middlebrook, A. M.,
582 Kolb, C. E., Baltensperger, U., and Worsnop, D. R.: Evolution of organic aerosols in the atmosphere, *Science*, 326, 1525-
583 1529, 10.1126/science.1180353, 2009.
- 584 Kontkanen, J., Deng, C., Fu, Y., Dada, L., Zhou, Y., Cai, J., Dällenbach, K. R., Hakala, S., Kokkonen, T. V., Lin, Z., Liu, Y.,
585 Wang, Y., Yan, C., Petäjä, T., Jiang, J., Kulmala, M., and Paasonen, P., 10.5194/acp-2020-215, 2020.
- 586 Kulmala, M., Dada, L., Daellenbach, K. R., Yan, C., Stolzenburg, D., Kontkanen, J., Ezhova, E., Hakala, S., Tuovinen, S.,
587 Kokkonen, T. V., Kurppa, M., Cai, R., Zhou, Y., Yin, R., Baalbaki, R., Chan, T., Chu, B., Deng, C., Fu, Y., Ge, M., He, H.,
588 Heikkinen, L., Junninen, H., Liu, Y., Lu, Y., Nie, W., Rusanen, A., Vakkari, V., Wang, Y., Yang, G., Yao, L., Zheng, J.,
589 Kujansuu, J., Kangasluoma, J., Petaja, T., Paasonen, P., Jarvi, L., Worsnop, D., Ding, A., Liu, Y., Wang, L., Jiang, J., Bianchi,



- 592 F., and Kerminen, V. M.: Is reducing new particle formation a plausible solution to mitigate particulate air pollution in Beijing
593 and other Chinese megacities?, *Faraday Discuss.*, 226, 334-347, 10.1039/d0fd00078g, 2021.
- 594 Lack, D. A., and Langridge, J. M.: On the attribution of black and brown carbon light absorption using the Ångström exponent,
595 *Atmospheric Chemistry and Physics*, 13, 10535-10543, 10.5194/acp-13-10535-2013, 2013.
- 596 Laskin, A., Laskin, J., and Nizkorodov, S. A.: Chemistry of atmospheric brown carbon, *Chem Rev.*, 115, 4335-4382,
597 10.1021/cr5006167, 2015.
- 598 Le Breton, M., Wang, Y., Hallquist, Å. M., Pathak, R. K., Zheng, J., Yang, Y., Shang, D., Glasius, M., Bannan, T. J., Liu, Q.,
599 Chan, C. K., Percival, C. J., Zhu, W., Lou, S., Topping, D., Wang, Y., Yu, J., Lu, K., Guo, S., Hu, M., and Hallquist, M.:
600 Online gas- and particle-phase measurements of organosulfates, organosulfonates and nitrooxy organosulfates in Beijing
601 utilizing a FIGAERO ToF-CIMS, *Atmospheric Chemistry and Physics*, 18, 10355-10371, 10.5194/acp-18-10355-2018, 2018.
- 602 Lelieveld, J., Evans, J. S., Fnais, M., Giannadaki, D., and Pozzer, A.: The contribution of outdoor air pollution sources to
603 premature mortality on a global scale, *Nature*, 525, 367-371, 10.1038/nature15371, 2015.
- 604 Lim, S., Lee, M., Kim, S. W., Yoon, S. C., Lee, G., and Lee, Y. J.: Absorption and scattering properties of organic carbon
605 versus sulfate dominant aerosols at Gosan climate observatory in Northeast Asia, *Atmos. Chem. Phys.*, 14, 7781-7793,
606 10.5194/acp-14-7781-2014, 2014.
- 607 Lim, Y. B., Tan, Y., Perri, M. J., Seitzinger, S. P., and Turpin, B. J.: Aqueous chemistry and its role in secondary organic
608 aerosol (SOA) formation, *Atmospheric Chemistry and Physics*, 10, 10521-10539, 10.5194/acp-10-10521-2010, 2010.
- 609 Lin, P., Rincon, A. G., Kalberer, M., and Yu, J. Z.: Elemental Composition of HULIS in the Pearl River Delta Region, China:
610 Results Inferred from Positive and Negative Electrospray High Resolution Mass Spectrometric Data, *Environmental Science
& Technology*, 46, 7454-7462, 10.1021/es300285d, 2012.
- 611 Liu, Q., Baumgartner, J., Zhang, Y., and Schauer, J. J.: Source apportionment of Beijing air pollution during a severe winter
612 haze event and associated pro-inflammatory responses in lung epithelial cells, *Atmospheric Environment*, 126, 28-35,
613 <https://doi.org/10.1016/j.atmosenv.2015.11.031>, 2016.
- 614 Liu, S., Aiken, A. C., Gorkowski, K., Dubey, M. K., Cappa, C. D., Williams, L. R., Herndon, S. C., Massoli, P., Fortner, E.
615 C., Chhabra, P. S., Brooks, W. A., Onasch, T. B., Jayne, J. T., Worsnop, D. R., China, S., Sharma, N., Mazzoleni, C., Xu, L.,
616 Ng, N. L., Liu, D., Allan, J. D., Lee, J. D., Fleming, Z. L., Mohr, C., Zotter, P., Szidat, S., and Prevot, A. S. H.: Enhanced
617 light absorption by mixed source black and brown carbon particles in UK winter, *Nat Commun.*, 6, 8435,
618 10.1038/ncomms9435, 2015.
- 619 Liu, T., Clegg, S. L., and Abbatt, J. P. D.: Fast oxidation of sulfur dioxide by hydrogen peroxide in deliquesced aerosol
620 particles, *Proceedings of the National Academy of Sciences*, 10.1073/pnas.1916401117, 2020a.
- 621 Liu, Y., Zhang, Y., Lian, C., Yan, C., Feng, Z., Zheng, F., Fan, X., Chen, Y., Wang, W., Chu, B., Wang, Y., Cai, J., Du, W.,
622 Daellenbach, K. R., Kangasluoma, J., Bianchi, F., Kujansuu, J., Petäjä, T., Wang, X., Hu, B., Wang, Y., Ge, M., He, H., and
623 Kulmala, M.: The promotion effect of nitrous acid on aerosol formation in wintertime in Beijing: the possible contribution of
624 traffic-related emissions, *Atmospheric Chemistry and Physics*, 20, 13023-13040, 10.5194/acp-20-13023-2020, 2020b.
- 625 Lopez-Hilfiker, F. D., Mohr, C., Ehn, M., Rubach, F., Kleist, E., Wildt, J., Mentel, T. F., Lutz, A., Hallquist, M., Worsnop,
626 D., and Thornton, J. A.: A novel method for online analysis of gas and particle composition: description and evaluation of a
627 Filter Inlet for Gases and AEROSols (FIGAERO), *Atmospheric Measurement Techniques*, 7, 983-1001, 10.5194/amt-7-983-
628 2014, 2014.
- 629 Lu, K., Fuchs, H., Hofzumahaus, A., Tan, Z., Wang, H., Zhang, L., Schmitt, S. H., Rohrer, F., Bohn, B., Broch, S., Dong, H.,
630 Gkatzelis, G. I., Hohaus, T., Holland, F., Li, X., Liu, Y., Liu, Y., Ma, X., Novelli, A., Schlag, P., Shao, M., Wu, Y., Wu, Z.,
631 Zeng, L., Hu, M., Kiendler-Scharr, A., Wahner, A., and Zhang, Y.: Fast Photochemistry in Wintertime Haze: Consequences
632 for Pollution Mitigation Strategies, *Environmental Science & Technology*, 53, 10676-10684, 10.1021/acs.est.9b02422, 2019.
- 633 Middlebrook, A. M., Bahreini, R., Jimenez, J. L., and Canagaratna, M. R.: Evaluation of Composition-Dependent Collection
634 Efficiencies for the Aerodyne Aerosol Mass Spectrometer using Field Data, *Aerosol Science and Technology*, 46, 258-271,
635 10.1080/02786826.2011.620041, 2012.
- 636 Mohr, C., Lopez-Hilfiker, F. D., Zotter, P., Prevot, A. S., Xu, L., Ng, N. L., Herndon, S. C., Williams, L. R., Franklin, J. P.,
637 Zahniser, M. S., Worsnop, D. R., Knighton, W. B., Aiken, A. C., Gorkowski, K. J., Dubey, M. K., Allan, J. D., and Thornton,
638 J. A.: Contribution of nitrated phenols to wood burning brown carbon light absorption in Detling, United Kingdom during
639 winter time, *Environ Sci Technol.*, 47, 6316-6324, 10.1021/es400683v, 2013.
- 640 Molteni, U., Bianchi, F., Klein, F., El Haddad, I., Frege, C., Rossi, M. J., Dommen, J., and Baltensperger, U.: Formation of
641 highly oxygenated organic molecules from aromatic compounds, *Atmospheric Chemistry and Physics*, 18, 1909-1921,
642 10.5194/acp-18-1909-2018, 2018.
- 643 Müller, M., Eichler, P., D'Anna, B., Tan, W., and Wisthaler, A.: Direct Sampling and Analysis of Atmospheric Particulate
644 Organic Matter by Proton-Transfer-Reaction Mass Spectrometry, *Analytical Chemistry*, 89, 10889-10897,
645 10.1021/acs.analchem.7b02582, 2017.



- 647 Ng, N. L., Canagaratna, M. R., Jimenez, J. L., Zhang, Q., Ulbrich, I. M., and Worsnop, D. R.: Real-Time Methods for
648 Estimating Organic Component Mass Concentrations from Aerosol Mass Spectrometer Data, *Environmental Science &*
649 *Technology*, 45, 910-916, 10.1021/es102951k, 2011.
- 650 Riipinen, I., Yli-Juuti, T., Pierce, J. R., Petäjä, T., Worsnop, D. R., Kulmala, M., and Donahue, N. M.: The contribution of
651 organics to atmospheric nanoparticle growth, *Nature Geoscience*, 5, 453-458, 10.1038/ngeo1499, 2012.
- 652 Sandradewi, J., Prévôt, A. S. H., Szidat, S., Perron, N., Alfarra, M. R., Lanz, V. A., Weingartner, E., and Baltensperger, U.:
653 Using Aerosol Light Absorption Measurements for the Quantitative Determination of Wood Burning and Traffic Emission
654 Contributions to Particulate Matter, *Environmental Science & Technology*, 42, 3316-3323, 10.1021/es702253m, 2008.
- 655 Schauer, J. J., Kleeman, M. J., Cass, G. R., and Simoneit, B. R. T.: Measurement of Emissions from Air Pollution Sources. 4.
656 C1-C27 Organic Compounds from Cooking with Seed Oils, *Environmental Science & Technology*, 36, 567-575,
657 10.1021/es002053m, 2002.
- 658 Siegel, K., Karlsson, L., Zieger, P., Baccharini, A., Schmale, J., Lawler, M., Salter, M., Leck, C., Ekman, A. M. L., Riipinen,
659 I., and Mohr, C.: Insights into the molecular composition of semi-volatile aerosols in the summertime central Arctic Ocean
660 using FIGAERO-CIMS, *Environmental Science: Atmospheres*, 10.1039/d0ea00023j, 2021.
- 661 Simoneit, B. R. T., Schauer, J. J., Nolte, C. G., Oros, D. R., Elias, V. O., Fraser, M. P., Rogge, W. F., and Cass, G. R.:
662 Levoglucosan, a tracer for cellulose in biomass burning and atmospheric particles, *Atmospheric Environment*, 33, 173-182,
663 [https://doi.org/10.1016/S1352-2310\(98\)00145-9](https://doi.org/10.1016/S1352-2310(98)00145-9), 1999.
- 664 Song, S., Gao, M., Xu, W., Sun, Y., Worsnop, D. R., Jayne, J. T., Zhang, Y., Zhu, L., Li, M., Zhou, Z., Cheng, C., Lv, Y.,
665 Wang, Y., Peng, W., Xu, X., Lin, N., Wang, Y., Wang, S., Munger, J. W., Jacob, D., and McElroy, M. B.: Possible
666 heterogeneous hydroxymethanesulfonate (HMS) chemistry in northern China winter haze and implications for rapid sulfate
667 formation, *Atmospheric Chemistry and Physics Discussions*, 1-26, 10.5194/acp-2018-1015, 2018.
- 668 Sun, Y., Wang, Z. F., Fu, P. Q., Yang, T., Jiang, Q., Dong, H. B., Li, J., and Jia, J. J.: Aerosol composition, sources and
669 processes during wintertime in Beijing, China, *Atmospheric Chemistry and Physics*, 13, 4577-4592, 10.5194/acp-13-4577-
670 2013, 2013.
- 671 Sun, Y., Du, W., Wang, Q., Zhang, Q., Chen, C., Chen, Y., Chen, Z., Fu, P., Wang, Z., Gao, Z., and Worsnop, D. R.: Real-
672 Time Characterization of Aerosol Particle Composition above the Urban Canopy in Beijing: Insights into the Interactions
673 between the Atmospheric Boundary Layer and Aerosol Chemistry, *Environ Sci Technol*, 49, 11340-11347,
674 10.1021/acs.est.5b02373, 2015.
- 675 Sun, Y., Du, W., Fu, P., Wang, Q., Li, J., Ge, X., Zhang, Q., Zhu, C., Ren, L., Xu, W., Zhao, J., Han, T., Worsnop, D. R., and
676 Wang, Z.: Primary and secondary aerosols in Beijing in winter: sources, variations and processes, *Atmospheric Chemistry*
677 *and Physics*, 16, 8309-8329, 10.5194/acp-16-8309-2016, 2016.
- 678 Tao, J., Surapipith, V., Han, Z., Prapamontol, T., Kawichai, S., Zhang, L., Zhang, Z., Wu, Y., Li, J., Li, J., Yang, Y., and
679 Zhang, R.: High mass absorption efficiency of carbonaceous aerosols during the biomass burning season in Chiang Mai of
680 northern Thailand, *Atmospheric Environment*, 240, 117821, <https://doi.org/10.1016/j.atmosenv.2020.117821>, 2020.
- 681 Teich, M., van Pinxteren, D., Wang, M., Kecorius, S., Wang, Z., Müller, T., Močnik, G., and Herrmann, H.: Contributions of
682 nitrated aromatic compounds to the light absorption of water-soluble and particulate brown carbon in different atmospheric
683 environments in Germany and China, *Atmospheric Chemistry and Physics*, 17, 1653-1672, 10.5194/acp-17-1653-2017, 2017.
- 684 Thornton, J. A., Mohr, C., Schobesberger, S., D'Ambro, E. L., Lee, B. H., and Lopez-Hilfiker, F. D.: Evaluating Organic
685 Aerosol Sources and Evolution with a Combined Molecular Composition and Volatility Framework Using the Filter Inlet for
686 Gases and Aerosols (FIGAERO), *Accounts of Chemical Research*, 53, 1415-1426, 10.1021/acs.accounts.0c00259, 2020.
- 687 Virkkula, A., Chi, X., Ding, A., Shen, Y., Nie, W., Qi, X., Zheng, L., Huang, X., Xie, Y., Wang, J., Petäjä, T., and Kulmala,
688 M.: On the interpretation of the loading correction of the aethalometer, *Atmospheric Measurement Techniques*, 8, 4415-4427,
689 10.5194/amt-8-4415-2015, 2015.
- 690 Vu, T. V., Delgado-Saborit, J. M., and Harrison, R. M.: Review: Particle number size distributions from seven major sources
691 and implications for source apportionment studies, *Atmospheric Environment*, 122, 114-132,
692 10.1016/j.atmosenv.2015.09.027, 2015.
- 693 Wang, J., Nie, W., Cheng, Y., Shen, Y., Chi, X., Wang, J., Huang, X., Xie, Y., Sun, P., Xu, Z., Qi, X., Su, H., and Ding, A.:
694 Light absorption of brown carbon in eastern China based on 3-year multi-wavelength aerosol optical property observations
695 and an improved absorption Ångström exponent segregation method, *Atmospheric Chemistry and Physics*, 18, 9061-9074,
696 10.5194/acp-18-9061-2018, 2018.
- 697 Wang, J., Liu, D., Ge, X., Wu, Y., Shen, F., Chen, M., Zhao, J., Xie, C., Wang, Q., Xu, W., Zhang, J., Hu, J., Allan, J., Joshi,
698 R., Fu, P., Coe, H., and Sun, Y.: Characterization of black carbon-containing fine particles in Beijing during wintertime,
699 *Atmospheric Chemistry and Physics*, 19, 447-458, 10.5194/acp-19-447-2019, 2019a.
- 700 Wang, J., Ye, J., Zhang, Q., Zhao, J., Wu, Y., Li, J., Liu, D., Li, W., Zhang, Y., Wu, C., Xie, C., Qin, Y., Lei, Y., Huang, X.,
701 Guo, J., Liu, P., Fu, P., Li, Y., Lee, H. C., Choi, H., Zhang, J., Liao, H., Chen, M., Sun, Y., Ge, X., Martin, S. T., and Jacob,



- 702 D. J.: Aqueous production of secondary organic aerosol from fossil-fuel emissions in winter Beijing haze, Proceedings of the
703 National Academy of Sciences, 118, e2022179118, 10.1073/pnas.2022179118, 2021a.
- 704 Wang, W., Liu, M., Wang, T., Song, Y., Zhou, L., Cao, J., Hu, J., Tang, G., Chen, Z., Li, Z., Xu, Z., Peng, C., Lian, C., Chen,
705 Y., Pan, Y., Zhang, Y., Sun, Y., Li, W., Zhu, T., Tian, H., and Ge, M.: Sulfate formation is dominated by manganese-catalyzed
706 oxidation of SO₂ on aerosol surfaces during haze events, *Nat Commun*, 12, 1993, 10.1038/s41467-021-22091-6, 2021b.
- 707 Wang, X. K., Hayeck, N., Brüggemann, M., Yao, L., Chen, H. F., Zhang, C., Emmelin, C., Chen, J. M., George, C., and Wang,
708 L.: Chemical Characteristics of Organic Aerosols in Shanghai: A Study by Ultrahigh-Performance Liquid Chromatography
709 Coupled With Orbitrap Mass Spectrometry, *Journal of Geophysical Research-Atmospheres*, 122, 11703-11722,
710 10.1002/2017jd026930, 2017.
- 711 Wang, Y., Hu, M., Wang, Y., Zheng, J., Shang, D., Yang, Y., Liu, Y., Li, X., Tang, R., Zhu, W., Du, Z., Wu, Y., Guo, S.,
712 Wu, Z., Lou, S., Hallquist, M., and Yu, J. Z.: The formation of nitro-aromatic compounds under high NO_x and anthropogenic
713 VOC conditions in urban Beijing, China, *Atmospheric Chemistry and Physics*, 19, 7649-7665, 10.5194/acp-19-7649-2019,
714 2019b.
- 715 Wang, Y., Chen, Y., Wu, Z., Shang, D., Bian, Y., Du, Z., Schmitt, S. H., Su, R., Gkatzelis, G. I., Schlag, P., Hohaus, T.,
716 Voliotis, A., Lu, K., Zeng, L., Zhao, C., Alfarrá, M. R., McFiggans, G., Wiedensohler, A., Kiendler-Scharr, A., Zhang, Y.,
717 and Hu, M.: Mutual promotion between aerosol particle liquid water and particulate nitrate enhancement leads to severe
718 nitrate-dominated particulate matter pollution and low visibility, *Atmospheric Chemistry and Physics*, 20, 2161-2175,
719 10.5194/acp-20-2161-2020, 2020.
- 720 Wu, C., Wu, D., and Yu, J. Z.: Quantifying black carbon light absorption enhancement with a novel statistical approach,
721 *Atmospheric Chemistry and Physics*, 18, 289-309, 10.5194/acp-18-289-2018, 2018.
- 722 Xie, C., Xu, W., Wang, J., Liu, D., Ge, X., Zhang, Q., Wang, Q., Du, W., Zhao, J., Zhou, W., Li, J., Fu, P., Wang, Z., Worsnop,
723 D., and Sun, Y.: Light absorption enhancement of black carbon in urban Beijing in summer, *Atmospheric Environment*, 213,
724 499-504, 10.1016/j.atmosenv.2019.06.041, 2019a.
- 725 Xie, C., Xu, W., Wang, J., Wang, Q., Liu, D., Tang, G., Chen, P., Du, W., Zhao, J., Zhang, Y., Zhou, W., Han, T., Bian, Q.,
726 Li, J., Fu, P., Wang, Z., Ge, X., Allan, J., Coe, H., and Sun, Y.: Vertical characterization of aerosol optical properties and
727 brown carbon in winter in urban Beijing, China, *Atmospheric Chemistry and Physics*, 19, 165-179, 10.5194/acp-19-165-2019,
728 2019b.
- 729 Yan, C., Yin, R., Lu, Y., Dada, L., Yang, D., Fu, Y., Kontkanen, J., Deng, C., Garmash, O., Ruan, J., Baalbaki, R., Schervish,
730 M., Cai, R., Bloss, M., Chan, T., Chen, T., Chen, Q., Chen, X., Chen, Y., Chu, B., Dällenbach, K., Foreback, B., He, X.,
731 Heikkinen, L., Jokinen, T., Junninen, H., Kangasluoma, J., Kokkonen, T., Kurppa, M., Lehtipalo, K., Li, H., Li, H., Li, X.,
732 Liu, Y., Ma, Q., Paasonen, P., Rantala, P., Pileci, R. E., Rusanen, A., Sarnela, N., Simonen, P., Wang, S., Wang, W., Wang,
733 Y., Xue, M., Yang, G., Yao, L., Zhou, Y., Kujansuu, J., Petäjä, T., Nie, W., Ma, Y., Ge, M., He, H., Donahue, N. M., Worsnop,
734 D. R., Veli-Matti, K., Wang, L., Liu, Y., Zheng, J., Kulmala, M., Jiang, J., and Bianchi, F.: The Synergistic Role of Sulfuric
735 Acid, Bases, and Oxidized Organics Governing New-Particle Formation in Beijing, *Geophysical Research Letters*, 48,
736 10.1029/2020gl091944, 2021.
- 737 Yang, F., Tan, J., Zhao, Q., Du, Z., He, K., Ma, Y., Duan, F., Chen, G., and Zhao, Q.: Characteristics of
738 PM_{2.5} speciation in representative megacities and across China, *Atmospheric Chemistry and Physics*,
739 11, 5207-5219, 10.5194/acp-11-5207-2011, 2011.
- 740 Yao, L., Fan, X., Yan, C., Kurten, T., Daellenbach, K. R., Li, C., Wang, Y., Guo, Y., Dada, L., Rissanen, M. P., Cai, J., Tham,
741 Y. J., Zha, Q., Zhang, S., Du, W., Yu, M., Zheng, F., Zhou, Y., Kontkanen, J., Chan, T., Shen, J., Kujansuu, J. T., Kangasluoma,
742 J., Jiang, J., Wang, L., Worsnop, D. R., Petaja, T., Kerminen, V. M., Liu, Y., Chu, B., He, H., Kulmala, M., and Bianchi, F.:
743 Unprecedented Ambient Sulfur Trioxide (SO₃) Detection: Possible Formation Mechanism and Atmospheric Implications,
744 *Environ Sci Technol Lett*, 7, 809-818, 10.1021/acs.estlett.0c00615, 2020.
- 745 Zhang, R., Jing, J., Tao, J., Hsu, S. C., Wang, G., Cao, J., Lee, C. S. L., Zhu, L., Chen, Z., Zhao, Y., and Shen, Z.: Chemical
746 characterization and source apportionment of PM_{_{2.5}} in Beijing: seasonal perspective, *Atmospheric Chemistry
747 and Physics*, 13, 7053-7074, 10.5194/acp-13-7053-2013, 2013.
- 748 Zhang, X., Lin, Y.-H., Surratt, J. D., Zotter, P., Prévôt, A. S. H., and Weber, R. J.: Light-absorbing soluble organic aerosol in
749 Los Angeles and Atlanta: A contrast in secondary organic aerosol, *Geophysical Research Letters*, 38, n/a-n/a,
750 10.1029/2011gl049385, 2011.
- 751 Zhang, Y., Favez, O., Canonaco, F., Liu, D., Močnik, G., Amodeo, T., Sciare, J., Prévôt, A. S. H., Gros, V., and Albinet, A.:
752 Evidence of major secondary organic aerosol contribution to lensing effect black carbon absorption enhancement, *npj Climate
753 and Atmospheric Science*, 1, 10.1038/s41612-018-0056-2, 2018.
- 754 Zhao, J., Qiu, Y., Zhou, W., Xu, W., Wang, J., Zhang, Y., Li, L., Xie, C., Wang, Q., Du, W., Worsnop, D. R., Canagaratna,
755 M. R., Zhou, L., Ge, X., Fu, P., Li, J., Wang, Z., Donahue, N. M., and Sun, Y.: Organic Aerosol Processing During Winter
756 Severe Haze Episodes in Beijing, *Journal of Geophysical Research: Atmospheres*, 124, 10248-10263, 10.1029/2019jd030832,
757 2019.

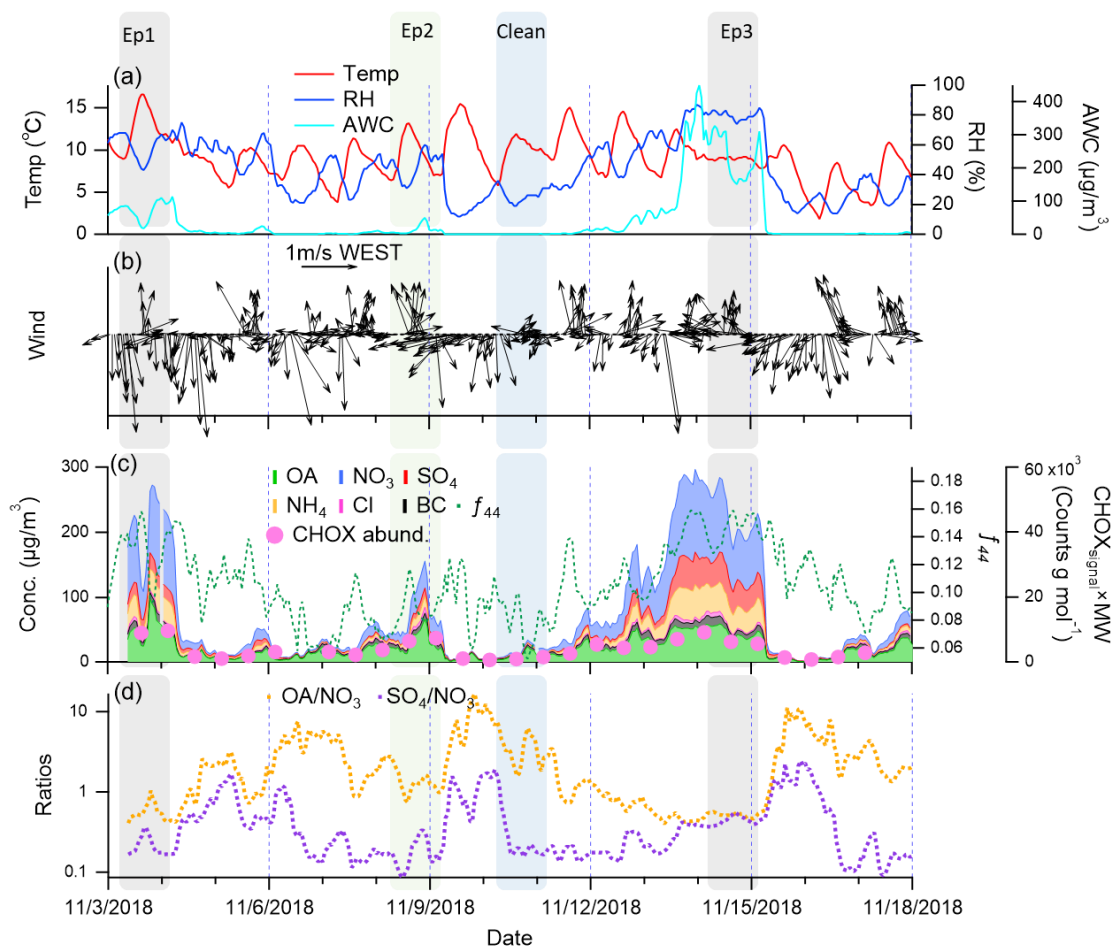


758 Zheng, Y., Chen, Q., Cheng, X., Mohr, C., Huang, W., Shi, X., Qiu, X., Ye, P., Zhu, T., Ge, Y., Liao, K., Miao, R., Fu, P.,
759 Chen, S., and Limin, Z.: Secondary organic aerosol formation under different haze conditions (to be submitted), 2021.
760 Zhou, Y., Dada, L., Liu, Y., Fu, Y., Kangasluoma, J., Chan, T., Yan, C., Chu, B., Daellenbach, K. R., Bianchi, F., Kokkonen,
761 T. V., Liu, Y., Kujansuu, J., Kerminen, V.-M., Petäjä, T., Wang, L., Jiang, J., and Kulmala, M.: Variation of size-segregated
762 particle number concentrations in wintertime Beijing, *Atmospheric Chemistry and Physics*, 20, 1201-1216, 10.5194/acp-20-
763 1201-2020, 2020.
764 Zotter, P., Herich, H., Gysel, M., El-Haddad, I., Zhang, Y., Močnik, G., Hüglin, C., Baltensperger, U., Szidat, S., and Prévôt,
765 A. S. H.: Evaluation of the absorption Ångström exponents for traffic and wood burning in the Aethalometer-based source
766 apportionment using radiocarbon measurements of ambient aerosol, *Atmospheric Chemistry and Physics*, 17, 4229-4249,
767 10.5194/acp-17-4229-2017, 2017.

768

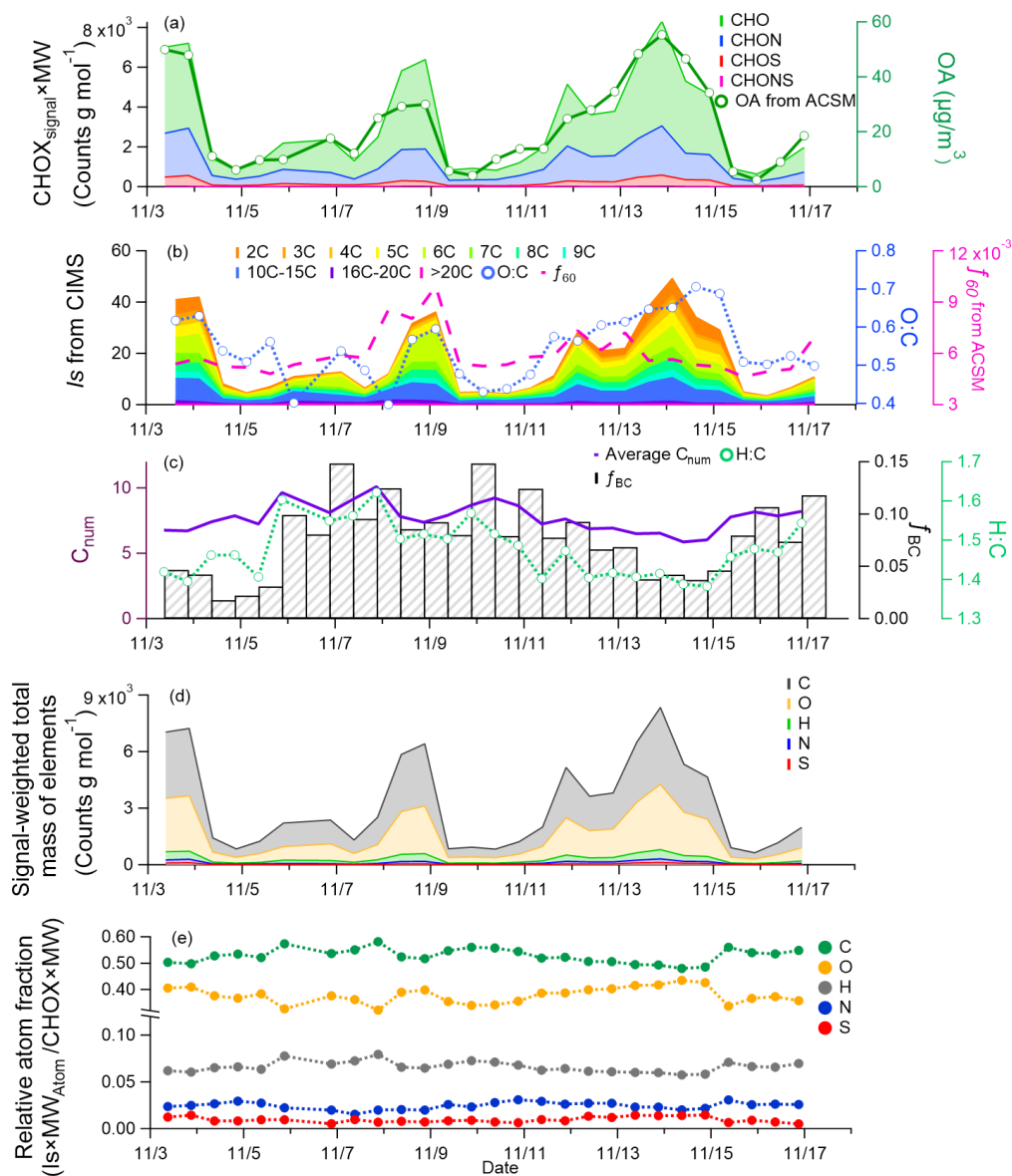


769



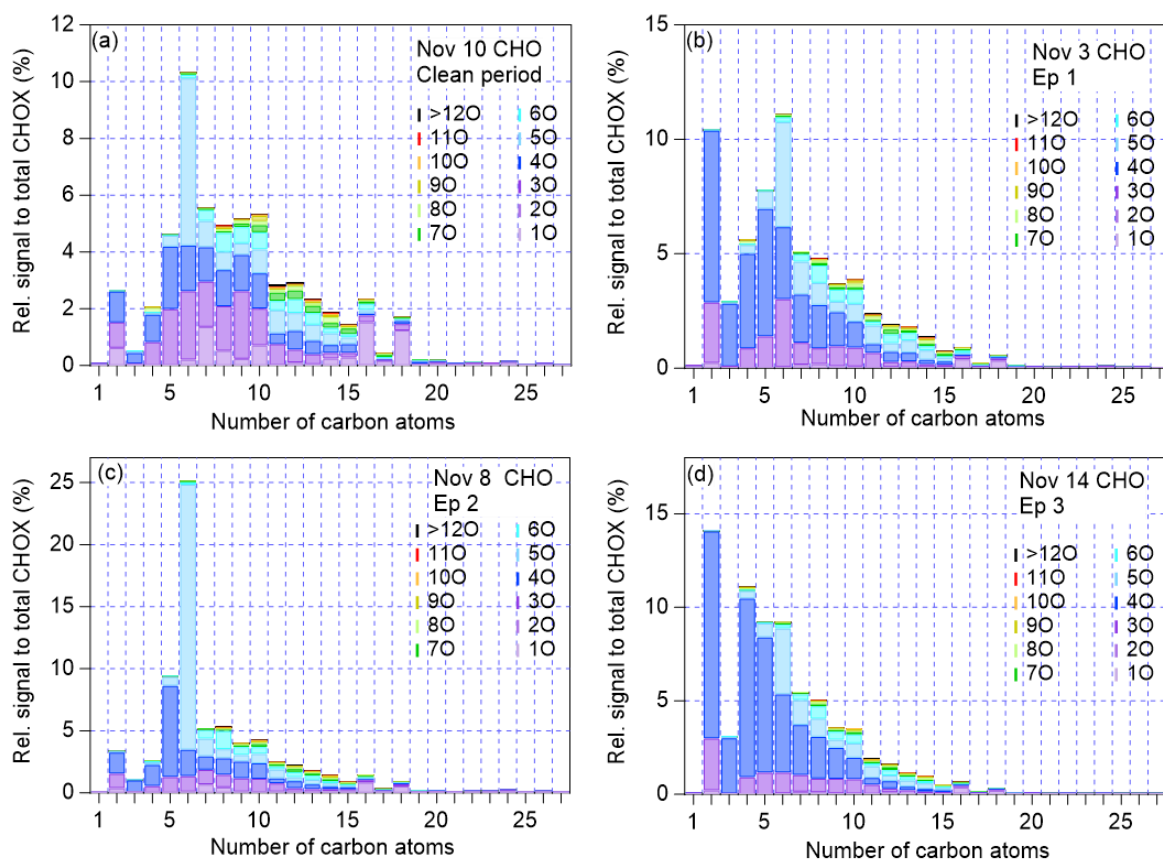
770

771 **Figure 1.** Time series of (a) temperature, relative humidity (RH), aerosol water content (AWC), (b) 1-hour averaged wind direction and
772 wind speed, (c) chemical components of NR-PM_{2.5}, BC, f_{44} from ACSM, CHOX abundance from FIGAERO-CIMS and their sampling
773 dates are marked by pink dots, (d) OA/NO₃ and SO₄/NO₃.



774

775 **Figure 2.** Time series of (a) abundance of CHO, CHON, CHOS, CHONS compounds, and OA concentrations measured by ACSM (b)
 776 signals of compounds grouped according to carbon number, O:C ratio, (c) average carbon number, H:C ratio, the fraction of BC to NR-
 777 PM_{2.5}+BC, and f₆₀ from ACSM, (d) the signal-weighted total mass of elements C, O, H, N, S, and (e) the relative atom fraction of C, O,
 778 H, N and S.



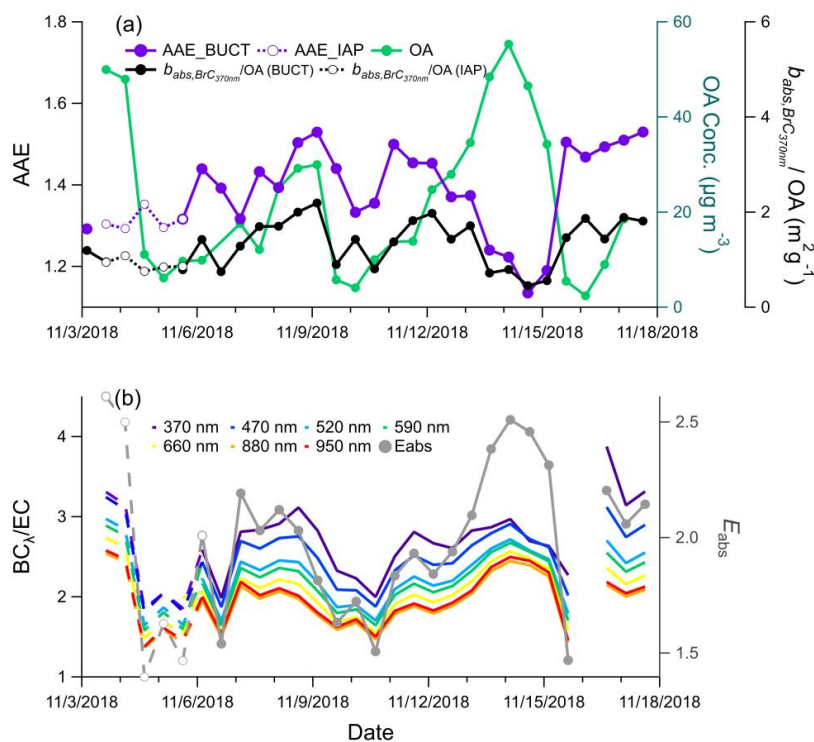
779

780 **Figure 3.** Signal fractions to total CHOX for CHO compounds with different numbers of oxygen and carbon atoms in (a) the clean period
781 (Nov 10), (b) Ep1 (Nov 3), (c) Ep2 (Nov 8) and (d) Ep3 (Nov 14) periods. The same plots for CHON compounds are displayed in Figure
782 S7.



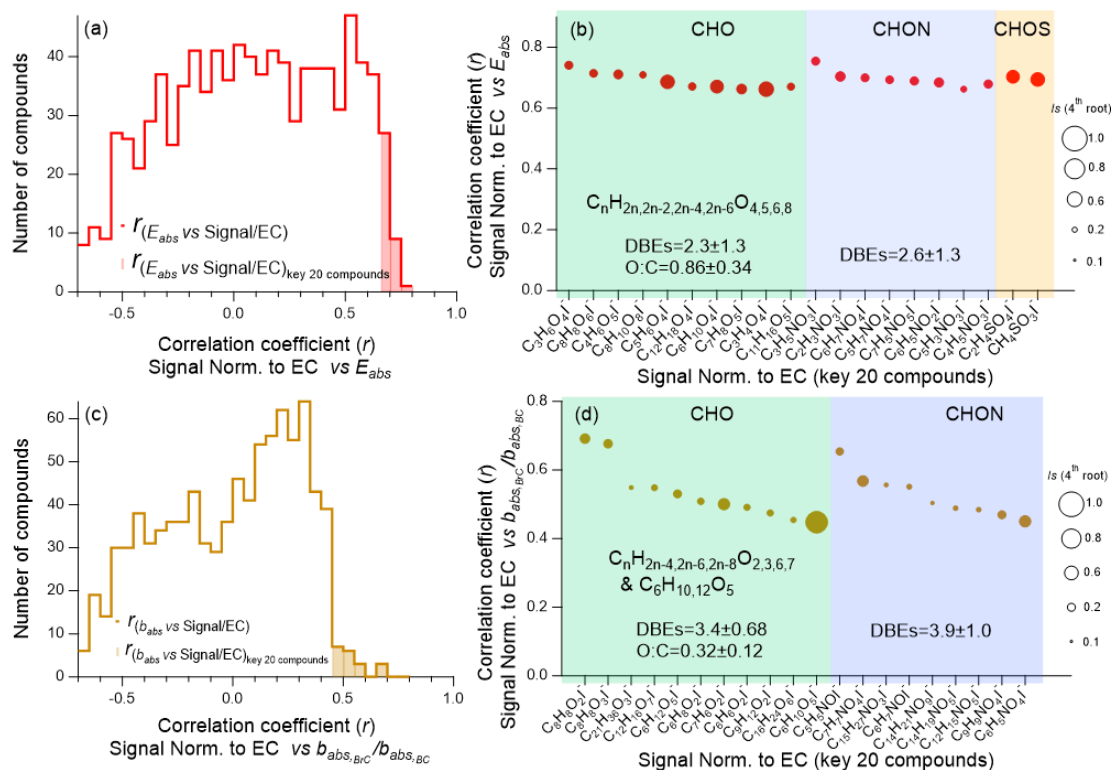
784

785 **Figure 4.** (a) Van Krevelen (VK) diagram of CHO compounds in the clean period (Nov 10), (b) VK diagram of CHON compounds in the
 786 clean period (Nov 10), (c) VK diagram of CHO compounds Ep1 (Nov 3), (d) VK diagram of CHON compounds in Ep1 (Nov 3), (e) VK
 787 diagram of CHO compound in Ep2 (Nov 8), (f) VK diagram of CHON compound in Ep2 (Nov 8), (g) VK diagrams of CHO compound in
 788 Ep3 (Nov 14), (h) VK diagram of CHON compound in Ep3 (Nov 14). Each dot represents an identified compound with its H/C and O/C
 789 ratios and color-coded by its DBEs. O/C ratios in CHO and CHON groups calculated from the atom numbers in the formulae. The size of
 790 symbols is proportional to the square root of the relative signal intensity of each compound. The same plot color-coded carbon number is
 791 shown in Figure S10.



792

793 **Figure 5.** (a) Time series of AAE, normalized $b_{\text{abs},\text{BrC}_{370\text{nm}}}$ (normalized to OA) and OA measured by ACSM during the sampling period,
 794 (b) ratio of BC to EC and E_{abs} calculated with $\text{BC}_{880\text{nm}}$ and EC. The solid lines represent the parameters measured at the BUCT site and
 795 dashed lines represent the parameters measured at the IAP site.



796

797

798

799

800

801

802

Figure 6. (a) Histogram of the correlation coefficients (r) between the normalized OA signals and E_{abs} at 880 nm for all identified compounds (red line) and the key 20 compounds (red shaded area), (b) the correlation coefficients of key 20 compounds for E_{abs} at 880 nm, (c) histogram of the correlation coefficients between the normalized OA compound signals and $b_{abs,BrC}/b_{abs,BC}$ at 370nm for all identified compounds (brown line) and the key 20 compounds (brown shaded area), and (d) the correlation coefficients of key 20 compounds for $b_{abs,BrC}/b_{abs,BC}$ at 370nm. The size of the symbols in (b) and (d) is proportional to the 4th root of the average signal intensities of the corresponding compound during the whole sampling period.

803

804